INAUGURAL – DISSERTATION
zur
Erlangung der Doktorwürde

der
Naturwissenschaftlich-Mathematischen
Gesamtfakultät

der
Ruprecht-Karls-Universität
Heidelberg

vorgelegt von
Christoph Johannes Meinrenken (M.S.E.)
aus Heidelberg

Tag der mündlichen Prüfung: 26. Juni, 2001

Simulation des physiologischen Kalziumsignals zur phasischen Transmitterfreisetzung an einer zentralen Synapse:
Kanal-Vesikel-Anordnung und ihre funktionelle Relevanz

Gutachter: Prof. Dr. Bert Sakmann (MPImF Heidelberg)
Prof. Dr. Heinz Horner (Universität Heidelberg)

Dissertation
submitted to the
Combined Faculties for the Natural Sciences and for Mathematics
of the Rupertus Carola University of
Heidelberg, Germany
for the degree of
Doctor of Natural Sciences

MODELING PHYSIOLOGICAL CALCIUM SIGNALING FOR FAST TRANSMITTER RELEASE AT A CENTRAL SYNAPSE: TOPOGRAPHY OF RELEASE SITES AND ITS FUNCTIONAL SIGNIFICANCE

presented by
Christoph Johannes Meinrenken (M.S.E.)
born in Heidelberg, Germany

Heidelberg, June 26, 2001

Referees: Prof. Dr. Bert Sakmann (MPImF Heidelberg)
Prof. Dr. Heinz Horner (Universität Heidelberg)

Zusammenfassung

SIMULATION DES PHYSIOLOGISCHEN KALZIUM - SIGNALS ZUR PHASISCHEN TRANSMITTERFREISETZUNG AN EINER ZENTRALEN SYNAPSE:
KANAL - VESIKEL - ANORDNUNG UND IHRE FUNKTIONELLE RELEVANZ

Diese Dissertation untersucht die räumliche Anordnung von Kalziumkanälen und Transmittervesikeln bei der Steuerung von schneller synaptischer Übertragung im Zentralnervensystem (Kanal-Vesikel-Topographie). Die klassische Fragestellung wurde in einer Reihe früherer Arbeiten untersucht, allerdings verhinderte die große Anzahl nur unzureichend bekannter Parameter die Klärung der Frage, welche Topographie die präsynaptische Kalzium-Signalgebung und damit die Übertragungseigenschaften zentraler Synapsen kontrolliert. Die vorliegende Arbeit verbindet ein detailliertes Computermodell mit neuen Interpretationen einer Vielzahl experimenteller Daten der Riesensynapse *Calyx of Held*. Die Arbeit beantwortet folgende Fragen: In welchem Abstand zueinander sind Kalziumkanäle angeordnet? Welche Amplitude, welches räumliche Profil und welcher zeitliche Verlauf zeichnen das präsynaptische Kalziumsignal aus? Sind Kalziumkanäle zufällig angeordnet oder gehorchen sie funktionsrelevanten Regeln, wie beispielsweise einer Anhäufung in Clustern? Wie viele Kanäle kontrollieren die Fusion eines einzelnen Vesikels, und schließlich, wo befinden sich diese Kanäle relativ zu dem Vesikel? Als quantitative Modellstudie liefert die Arbeit neue Erkenntnisse über Praktikabilität und Gültigkeit der Simulation von Kalziumdiffusion und -pufferung in Nervenzellen. Als physiologische Studie klärt sie gleichzeitig, welche topographischen Eigenschaften dieser Synapse ihre spezielle Funktion erst ermöglichen und warum.

Abstract

MODELING PHYSIOLOGICAL CALCIUM SIGNALING FOR FAST
TRANSMITTER RELEASE AT A CENTRAL SYNAPSE:
TOPOGRAPHY OF RELEASE SITES AND ITS FUNCTIONAL SIGNIFICANCE

This thesis addresses how calcium channels and neurotransmitter vesicles at release sites are spatially organized to control fast synaptic transmission in the central nervous system (topography of release sites). The problem, investigated here for the giant synapse calyx of Held, has been addressed before by a number of studies. However, the large number of poorly known parameters has often defeated attempts to conclude which topography governs presynaptic calcium signaling and thus the transmission characteristics of central synapses. Combining a computer model of buffered calcium diffusion and release with novel analyses of available experimental data, this work answers the following questions: What is the distance between individual calcium channels at release sites? What are the amplitude, spatial profile, and time course of the $[Ca^{2+}]$ signal controlling phasic release? Are channels located randomly or following functional organizing principles, such as clustering? How many channels control the fusion of individual vesicles? And finally, where are these channels located with respect to the vesicles? While providing new insights into prerequisites and feasibility of buffered calcium-diffusion modeling in nerve cells, a particular aim of this study is to clarify the significance of crucial aspects of the topography for the specific physiological function of the synapse.

Acknowledgments

My advisor, Bert Sakmann, for his continuous support and advice. Herr Sakmann has created a wonderful laboratory, with an atmosphere of mutual respect and support, and a great environment to do scientific work in.

My co-advisor, Heinz Horner for his time and professional advice.

Gerard Borst, who taught me pretty much all there is to know about the calyx of Held synapse. His teaching of electrophysiological techniques and mechanisms of synaptic transmission meant a fascinating and scientifically rigorous introduction to neuroscience.

Erwin Neher, for help, advice, and for sharing his abundant experience in similar work.

Everyone in the department of cell physiology at the Max Planck Institute for Medical Research (Heidelberg), for countless discussions and for the help without which this work would not have been possible.

Table of contents

List of figures

List of tables

List of equations

A. INTRODUCTION

A.1. OBJECTIVE OF THIS STUDY

During fast synaptic transmission, the release of neurotransmitter from vesicles in the presynaptic terminal is controlled by calcium (Katz, 1969). Brief influxes of calcium ions through voltage gated channels cause a transient rise in the intracellular concentration of calcium ions ([Ca^{2+}]). Within less than a millisecond, this rise in [Ca^{2+}] causes vesicles to fuse with the terminal membrane, releasing neurotransmitter. Since calcium ions inside the terminal diffuse away from the calcium channels, the rise in [Ca^{2+}] is less pronounced with increasing distance from the channels. Therefore, the release process cannot work at all locations on the membrane. Instead, a vesicle (i.e. the release controlling molecular sensor) must be located sufficiently close to one or more calcium channels (Augustine and Neher, 1992). The exact distance between vesicles and channels critically determines time course and amplitude of the [Ca^{2+}] signal at the vesicles, and thus the time course of phasic transmitter release (Barrett and Stevens, 1972; Zucker and Stockbridge, 1983). Therefore, understanding the functional and spatial organization of vesicles relative to release controlling channels (henceforth: topography of release sites) is crucial to our understanding of phasic transmitter release itself.

A.1.1. Previous, related studies

Historically, there have been three lines of approach to investigate the topography of release sites of different types of synapses of the nervous system.

(1) *Imaging of the local calcium signals evoked by calcium channels at release sites*. The rise and decay of [Ca^{2+}] around single channels, so called 'calcium domains', is very fast (tens of microseconds) and along very steep spatial gradients (tens of nanometers; Neher, 1998a). This is beyond the resolution of current imaging techniques. Although several studies have shown the existence of (sub micrometer) regions of locally elevated [Ca^{2+}] at presynaptic release sites, their spatio-temporal resolution was too low to identify calcium domains of individual channels (Llinas et al., 1992; Tucker and Fettiplace, 1995; DiGregorio et al., 1999; Sugimori et al., 1994; Roberts et al., 1990).

(2) *Direct imaging of both vesicles and calcium channels at the release sites of synapses*. For example, it has been possible to visualize the spatial organization of vesicles and channels at the frog neuromuscular junction (electron microscopy, Harlow et al., 2001). However, such

data is not yet available for central synapses like the one we investigate here. Although the location of vesicles at presynaptic release sites have been determined by electron microscopy (Lübke et al., 2001), the simultaneous imaging of vesicles and calcium channels has not yet been possible. Therefore, for the central synapse we investigate in this study, the location of vesicles relative to calcium channels is unknown.

(3) *Experimental data combined with numerical simulations*. Since neither measurements of the 'calcium domains' nor direct imaging of the location of calcium channels are available, the understanding of the local [Ca^{2+}] dynamics during action potentials must rely on experimental data on transmitter release and on quantitative models (Neher, 1998b). A number of studies have investigated the significance of vesicle/channel location (Zucker and Fogelson, 1986; Cooper et al., 1996; Gil et al., 2000), some of them quantifying transmitter release based on measured calcium sensitivity of the release controlling molecular sensor (Chow et al., 1994; Klingauf and Neher, 1997; Bertram et al., 1999; Bennett et al., 2000). However, the considerable number of poorly known parameters in the models often has defeated attempts to conclude with certainty the topography of release sites (Neher, 1998b).

A.1.2. Aim and focus of this study

Here, we present a model which simulates the physiological [Ca^{2+}] signal and subsequent phasic transmitter release for the calyx of Held, a presynaptic giant terminal located in the Medial Nucleus of the Trapezoid Body (MNTB) of mammalian brainstem. The model is based on a large body of experimental data which constrain key parameters of the quantitative simulations. The central aim of this study is to identify key characteristics of the topographic organization of release sites. Specifically, we will address the following questions: What is the distance between individual Ca^{2+} channels at release sites? What are the amplitude, spatial profile, and time course of the [Ca^{2+}] signal controlling phasic release? Are channels located randomly or following functional organizing principles, such as clustering? How many channels control the fusion of individual vesicles? And finally, where are these channels located with respect to the vesicles?

As will be shown in chapter B, the physiological processes governing neurotransmitter release form a very complex and highly non-linear quantitative model system. Consequently, the results of our model are often difficult to interpret and all but impossible to predict. By the same token, it is difficult to discriminate between factors crucial and less crucial for the

release of neurotransmitter at real synapses: Which of the aspects of the model make transmitter release "work" vs. which aspects of the model provide little more than a headache for the computer programmer?[1] To address this, chapter D focuses on the quantitative effects of crucial characteristics of the release site topography we found, and how these characteristics provide the synapse with crucial advantages facilitating its physiological function.

While our findings and the calculations we show are calibrated to the calyx of Held, our main conclusions are presented as general principles and may be applied to other fast synapses.

A.2. PHILOSOPHY OF APPROACH

The objective of this study is to determine the value of a parameter, by comparing the predictions of a quantitative model to experimental results. The "parameter", in our case, is the spatial organization of release controlling calcium channels and vesicles at release sites of the calyx of Held – the topography of its release sites. Our study, however, must not be considered an exercise in parameter fitting, for it lacks crucial prerequisites for such a procedure. The problem at hand lacks: (1) a quantitative model that *would* describe the experimentally measured results accurately, if all parameters *were* known (2) experimental data accurate enough to dismiss one set of parameters against another based on a discrepancy between prediction and experiment.

With respect to (1), we have to consider that the quantitative model we use in this study is an approximation. Although the three modules of the model – calcium influx through channels, buffered diffusion of calcium from channels to vesicles, and calcium sensitive release of neurotransmitter – capture the crucial steps of the real processes, they are not a fully accurate description thereof.[2] Therefore, any fitted parameter, e.g. the distance between a calcium channel and a vesicle, cannot be considered to be accurate either. With respect to (2), the

---

[1] The headaches, of course, are interesting to anyone working in biophysical modeling or similar fields. Working in a physiology department, however, I tried, in this work, to contribute to a physiologist's view as well.

[2] This is especially true for the calcium sensitive release model. In our study, we use, alternately, two kinetic models from two independent experimental studies (see section B.5). Both models represent a major advance in the knowledge of the sensitivity of neurotransmitter release at the calyx of Held synapse. However, the models ascribe different calcium sensitivities to the vesicles, and they imply different molecular mechanisms governing the release process.

available experimental data – although state of the art – show a common characteristic of biological data: Results of individual studies have considerable experimental uncertainty and results across different studies vary, sometimes to a degree of being inconsistent (see chapter A, Table C-1 and Table C-2).

In previous, similar modeling studies, the above problem was further aggravated: Not only was the topography of release sites unknown, but several other, crucial parameters in the models were not well known either (volume and shape of presynaptic terminal, capacity and kinetics of endogenous calcium buffers, and the calcium sensitivity of the release mechanism). Reviewing efforts to characterize the calcium signal for fast neurotransmitter release, Erwin Neher concluded: "The impact of our ignorance of many of these parameters cannot be overstated" (Neher, 1998b). In contrast to previous studies, the present work benefits from recent research which has determined the morphology of the calyx of Held as well as key parameters of the release process. These data, in combination with other experimental work, greatly reduce the uncertainty inherent in the previous studies.

Even after many of the key parameters have been measured, the above difficulties (1) and (2) remain. The topography of release sites *cannot* be determined by a straightforward parameter fit. Instead, we pursue the following approach: By detailed analyses of the experimental data and respective predictions of the model, we develop a set of 3 conclusions which characterize the topography of release sites (sections C.2, C.3, and C.4). As will be discussed in chapter E, all three conclusions are based on robust, quantitative effects, and were arrived at by scanning large parameter spaces of a multitude of hypothetical release site topographies.[3] Consistent with the above limitations (1) and (2), the conclusions do not, however, give exact values for the number of calcium channels or distances between channels and vesicles. Rather, the conclusions describe *properties* of spatial organization that release sites most likely feature in order to comply with the experimental data. These properties place constraints on the topography conceivably found at the real synapse. Our analyses are chosen such that combining the individual constraints forms a step by step exclusion process – a logical puzzle if you will – from which a specific topography of release sites emerges. The final result of our approach is a detailed concept of the release site topography most likely to be

[3] This includes a number of sensitivity analyses for poorly known parameters, see sections D.3 and E.1.1.

found at a real calyx of Held synapse – all the while avoiding the poor reliability of a straightforward parameter fit.

A.3. THE MODEL SYSTEM: CALYX OF HELD

We study the physiological calcium signal and release site topography of the calyx of Held, a presynaptic terminal located in the Medium Nucleus of the Trapezoid Body (MNTB) of mammalian[4] brainstem (Masterton et al., 1967). In recent years, this synapse has become an increasingly popular model system to study fast release of neurotransmitter. Due to its comparatively large size (circa 10 µm across), the synapse is easily visible under light microscopy and can be electrophysiologically accessed ("patched") on the presynaptic as well as on the postsynaptic side. Simultaneous recordings from the presynaptic and postsynaptic cell – at controlled membrane potentials and ionic conditions – have allowed researchers to gather detailed experimental data about the transmission characteristics of this synapse. The physiology of the calyx of Held as well as the experimental techniques relevant to our study have been described in detail elsewhere (e.g. Forsythe, 1994; Borst and Sakmann, 1996; Helmchen et al. 1997).

A giant-type terminal with a large volume (~ 400 μm^3), the calyx of Held combines 1000 - 2000 *release sites* into a single, presynaptic terminal. We define a release site as the functional unit of a releasable vesicle and one or several calcium channels controlling its release. The 1000 - 2000 release sites are located at ~ 600 *active zones*, electron-dense protein structures on the presynaptic membrane where vesicles may fuse with the membrane (dark spots in Figure B-1 A; see Table C-1 for detailed data on the morphology of the calyx of Held terminal). For readers unfamiliar with neuroscience, the following is a brief/simplified list of events during synaptic transmission, with particular attention to the concepts and terminoligy used throughout this thesis:

– a presynaptic *action potential* (a transient change of the trans-membrane voltage) reaches the terminal, causing a transient increase in the open probability of voltage-dependent *calcium channels*

[4] Of rat, in our case. (And, yes, humans have it, too.)

- calcium ions are driven through the open channels into the presynaptic terminal (along the electro-chemical gradient), causing a transient rise in the intracellular concentration of free calcium ($[Ca^{2+}]$)
- via a not yet fully identified mechanism, the transient rise of $[Ca^{2+}]$ near *releasable vesicles* (located at *active zones* on the presynaptic membrane) triggers a process which allows the vesicles to fuse with the membrane. The vesicular membrane forms a pore with the outer membrane of the terminal such that *neurotransmitter* (glutamate in our case) is released into the *presynaptic cleft*, the extra cellular space between presynaptic and postsynaptic cell
- the transmitter diffuses to the postsynaptic cell and causes the postsynaptic response. In experiments, the amount of released transmitter (in relative units) and the number of vesicles fused with the membrane (in absolute numbers) can be quantified by monitoring the postsynaptic response.[5] Note, however, that the postsynaptic response is not at the focus of this study.

To study the underlying mechanisms of synaptic transmission, the amount of transmitter released at the calyx of Held can be manipulated in various ways. Three of these are:

- *Reduction in the concentration of calcium ions in the extra cellular solution*. This results in a reduced influx through individual calcium channels, lower $[Ca^{2+}]$ transients, and thus in a reduced amount of released transmitter.
- *Reduction in the number of calcium channels that open during an action potential*. This results in a reduced calcium influx, lower $[Ca^{2+}]$ transients, and thus to reduced transmitter release.
- *Addition of exogenous calcium buffers to the pipette solution which is washed into the presynaptic cell*. This results in lower $[Ca^{2+}]$ transients, even if the influx of calcium through the channels remains the same. The result, again, is a reduction in the amount of released transmitter.

The above experimental manipulations are central to the findings of this study. Their simulation in the model will be explained in chapter B, respective experimental results and implications for the topography of release sites will be discussed in detail in chapter C. In

[5] For details, please see section B.5.4.

chapter D, we will demonstrate the significance of our findings on the topography for the transmission characteristics of this synapse: sustained, high fidelity transmission, at frequencies up to several hundred action potentials per second.

B. DESCRIPTION OF THE MODEL

B.1. ABOUT THIS CHAPTER

The primary objective of this study is to determine the topography of release sites at the calyx of Held synapse. To achieve this, this work makes extensive use of a quantitative model whose design was integral to the presented results. The model consists of three modules, quantifying the three key processes controlling neurotransmitter release at fast central synapses: (1) influx of calcium ions (Ca^{2+}) through voltage-gated channels (2) buffered diffusion of Ca^{2+} from the channels into the 3-dimensional terminal space, giving rise to a time-dependent 3-dimensional field of Ca^{2+}-concentrations (3) triggering of neurotransmitter release via a calcium-sensitive molecular release model.

The three modules will be described in detail in the following sections. It must be noted, that the quantitative concepts and equations governing the three above processes are well known and have been applied numerous times.[6] It is not the objective of this work to explain, comment on, or improve established techniques that quantify the above processes. Rather, the focus of the model-building and code-writing undertaken for this study – and with it the focus of this chapter – is the implementation and adaptation of the established techniques into a single, consistent model which quantifies physiological calcium signaling and transmitter release at the calyx of Held synapse. As will become apparent in chapter C, a particular challenge of designing the numerical simulations was to make them fast such that we could scan large parameter spaces of different hypothetical release site topographies. Therefore, chapter B includes a description of the various steps we undertook to reduce the number of computer operations – while avoiding any approximation that would have failed to capture crucial effects of physiological calcium signaling and its dependence on the topography of release sites.

B.2. IMPLEMENTATION OF TRUE MORPHOLOGY AS SIMPLIFIED SUB-COMPARTMENTS

B.2.1. Morphology of the calyx of Held terminal

Reconstructed from serial electron-microscopic section images (Figure B-1 C), the shape of the calyx of Held terminal resembles a hood-shaped structure that covers about half of the

[6] Respective references will be given below.

spherical post-synaptic cell (Figure B-1 A; Lübke et al., 2001).[7] The terminal has a volume of about 400 μm^3, a membrane surface area of about 2000 μm^2, and a thickness of 400 nm (= distance between the presynaptic membrane facing the synaptic cleft and the presynaptic membrane facing away from the cleft). The shape can be pictured as a thin quad that bends around and covers half of the post-synaptic cell (32 x 32 $\mu m^2 \approx 1000 \mu m^2$ bottom area with a height of 400 nm).

B.2.2. Sub-compartment as control volume for buffered diffusion simulations

Numerical simulations of buffered calcium diffusion for the *entire* terminal volume, though possible, would be very computationally expensive. Fortunately – in order to capture the crucial features of physiological calcium signaling and its dependence on the topography of release sites – simulations for the entire volume are not necessary. In fast releasing, central synapses such as the calyx of Held, the sites of release are confined to specialized regions on the presynaptic membrane, so called active zones. Per terminal, about 600 active zones can be identified (dark spots in Figure B-1 A). These are electron-dense, patch-like areas of the presynaptic membrane where releasable vesicles are located and the release process is triggered by the $[Ca^{2+}]$ transients. However, not only the release of vesicles is a localized event, the calcium signaling, i.e. the transient rise of $[Ca^{2+}]$ that triggers the release, is a *local* event as well (Augustine and Neher, 1992). The release of vesicles at active zones is controlled by calcium channels located at not more than several hundreds of nanometers away from the vesicle. Due to calcium diffusion and buffering, calcium channels further away, for example at far away active zones on the other side of the terminal, will only affect the volume average $[Ca^{2+}]$ in the terminal, not however the local $[Ca^{2+}]$ transients in the "vicinity" (~ hundreds of nanometers) of vesicles. Only these local $[Ca^{2+}]$ transients can trigger the release of transmitter. To capture the calcium signaling controlling release at a particular active zone, it is therefore sufficient to capture calcium channels and resulting calcium domains within hundreds of nanometers from that active zone. Note that this localization of calcium signaling, although anticipated in earlier theoretical work (Augustine and Neher, 1992), was confirmed, *not* presumed in the present work (see section B.2.2.2 as well as conclusion II, section C.3).

---

[7] Unless otherwise indicated, all reconstruction data and analyses on the morphology of the terminal was taken from Lübke et al., 2001.

When comparing the predictions of our model to experimental data, we must consider that experiments can only measure the combined release from all fused vesicles in the terminal, not release processes at individual active zones alone. Even though the model calculates buffered diffusion and release for one active zone, it can still capture effects of variations in the location of calcium channels and vesicles across active zones of the same terminal. The technical implementation of this effect into our model will be described in section B.5.3.

B.2.2.1. The sub-compartment: Quad around an active zone

The control volume for the numerical simulations is a quad, typically[8] with a bottom area of 525 x 525 nm^2 and a height of 400 nm (Figure B-1 D). 400 nm correspond to the average thickness of the terminal. The bottom of the quad is considered the presynaptic membrane facing the cleft, part of it active zone, with calcium channels and releasable vesicles at hypothesized locations (see chapter C). The control volume is sub-divided into voxels which determine the spatial resolution of the numerical simulations (explained in section B.4.6.1).

B.2.2.2. Inter-dependence of [Ca^{2+}] transients of different active zones

For most simulations, the control volume around an active zone is considered a closed space with boundary conditions such that there can be no flux of calcium through its walls (except for channels in the presynaptic membrane, i.e. in the bottom wall of the control volume). In this mode, the model simulates influx and buffered diffusion of calcium for a single sub-compartment, thus assuming that the local [Ca^{2+}] signaling in the vicinity of one active zone is independent of the calcium channels located at other active zones or anywhere in-between active zones in the un-specialized membrane (except for the effects of volume average [Ca^{2+}], see section B.2.2.3).

However, such independence of the [Ca^{2+}] transients at individual active zones is not *presumed* in all simulations. In section C.3, we also consider scenarios where the entire pre-synaptic membrane is covered with a regular grid of calcium channels, thus simulating the [Ca^{2+}] transients in the entire terminal. This is done by using a single control volume as described above, while applying periodic boundary conditions to the four side walls.

[8] In some scenarios, the exact dimensions of the control volume were different. See section B.2.2.3.

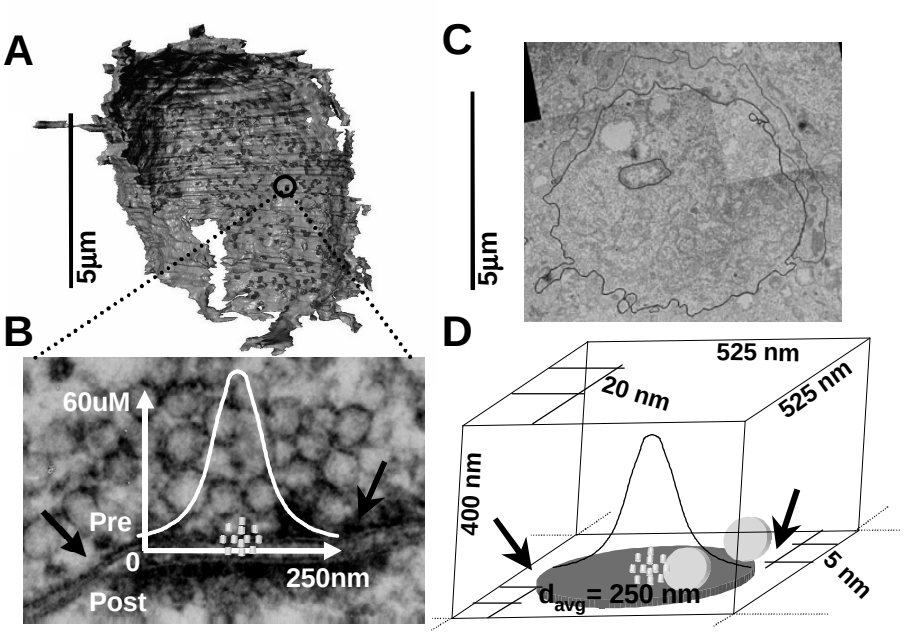

Figure B-1. Overview of morphology and model implementation.
(A) 3-dimensional reconstruction of a single calyx of Held terminal from serial EM-sections; dark spots identify active zones (AZ) (Lübke et al., 2001). (B) Detail study of a single EM-section showing an AZ cross-section with ~ 1-3 docked vesicles (vesicles not directly at membrane are not considered part of the readily releasable pool of vesicles). Superimposed: snap-shot of a $[Ca^{2+}]$ domain around a channel cluster at the time of peak I_{Ca} (same as trace 1 in Figure D-3 A). (C) Single EM-section with superimposed contour lines indicating the pre-synaptic membrane (top), the post-synaptic membrane (bottom), and the nucleus (small oval inside post-synaptic contour) (Lübke et al., 2001). (D) Dimensions of sub-compartments (not to scale) around individual AZ for which the buffered-diffusion scheme was calculated numerically (3-dim, full time course, no approximation on buffer saturation; see section B.4). As in B, channel cluster is at center of AZ for illustrative purposes only. Arrows identify borders of AZ. Partial grids indicate the spatial resolutions in different parts of the control volume.

B.2.2.3. Calcium influx into a sub-compartment vs. total influx into terminal

During physiological calcium signaling, the volume average $[Ca^{2+}]$ (spatial equilibrium following an action potential) crucially determines whether the release of neurotransmitter comes to a halt after a single action potential. The volume average $[Ca^{2+}]$ must be below the threshold to trigger any significant amount of release (for the calyx of Held about 1 µM; Bollmann et al., 2000). Therefore, our model must reflect volume average $[Ca^{2+}]$ correctly, even if it simulates $[Ca^{2+}]$ dynamics for a sub-compartment only. Correct quantification of volume average $[Ca^{2+}]$ also allows us to simulate the build up of $[Ca^{2+}]$ during high frequency synaptic transmission (section D.4.2).

In the cluster scenarios simulating physiological conditions (chapter D), the total influx entering a control volume (0.110 μm^3) is 0.26 fC or 12 µM un-buffered Ca^{2+}. Given the binding ratios of the endogenous buffers (section B.4.4), 12 µM un-buffered Ca^{2+} increases the volume

average [Ca^{2+}] in the control volume from 50 nM to 379 nM, the same increase as that observed in experiments (Table C-1). 600 sub-compartments (for 600 active zones) contribute a total of 0.16 pC Ca^{2+} (per action potential) which is 17% of the whole cell value observed in experiments. The "total" modeled volume (600 sub-compartments ~ 17% of 400 um^3) corresponds to this ratio. Therefore, the increase in volume average [Ca^{2+}] in the sub-compartment is the same as that experimentally observed for the whole terminal. This approach indirectly accounts for calcium that enters through other channels, located away from release sites, assuming that these channels do not (significantly) affect local [Ca^{2+}] transients at release sites but only volume average [Ca^{2+}] (for discussion, see section E.2.1).

To comply with the experimental measurement of volume average [Ca^{2+}], Δ[Ca^{2+}] is 12 μM in every scenario; whenever calcium influx for the control condition is changed (chapter C), the volume of the sub-compartment is changed accordingly.

B.2.2.4. *Advantages of sub-compartment design and validation by experiments*

Simulating the processes for a single sub-compartment rather than for the entire terminal offers several advantages:

- reduced computation time
- simplified geometry of control volume: presynaptic membrane around a single active zone is almost plane (curvature of membrane negligible), so that the control volume can be assumed as a quad with straight angels; the full morphology of the terminal would be a far more complicated structure
- the actual, exact values of membrane area, volume, and shape of the terminal (which are available only for a single, reconstructed cell) are not crucial to our results. Our model focuses on total calcium influx and volume average [Ca^{2+}], both of which have been measured for many terminals (Table C-1)
- in combination with our results on the topography of release sites, our design allows for direct estimates of the density of calcium channels on active zones versus that on the unspecialized presynaptic membrane (section D.1.4)

The design of our model – the focus on local [Ca^{2+}] signaling around individual active zones – is in agreement with a number of experimental studies. This will be discussed in section D.1.4 and in section E.2.1.

B.3. MODULE 1: INFLUX OF CALCIUM THROUGH CHANNELS IN THE MEMBRANE

To simulate the calcium influx through individual channels in response to action potentials, the model uses a standard, 2-gate Hodgkin-Huxley model, using parameters fitted for the calyx of Held. The channels' gates and the resulting currents are driven by action potential waveforms (Figure C-3 A). The governing equations and parameter values are given in Borst and Sakmann, 1998 (assume one channel type controlling the release, see discussion in section E.2.1). The only remaining free parameter is the single channel conductance (unknown for the calyx of Held). It is determined as explained in section C.1. In the model, the conductance is the same for all channels, but varies for different hypothesized topographies of channels and vesicles (values see chapter C). To simulate experiments with reduced $[Ca^{2+}]$ in the extracellular solution, channel conductance is reduced to match the reduction of whole cell I_{Ca} observed in experiments.

The Hodgkin-Huxley model predicts a time course of calcium current for each channel ($I_{Ca}(t)$). In the numerical simulation, this current determines the amount of Ca^{2+} (per time step)[9] added to every voxel that is located directly 'above' a hypothetical calcium channel in the membrane (calcium entry point). As the time course of I_{Ca} for each calcium entry point, simulations use either the time course of the whole cell calcium current (all calcium entry points are 'open' and each contributes the same $I_{Ca}(t)$ = average $I_{Ca}(t)$ predicted by Hodgkin-Huxley model). Or the model varies $I_{Ca}(t)$ for each calcium entry point stochastically (individual entry points contribute different $I_{Ca}(t)$; some remain 'closed'). Individual $I_{Ca}(t)$ are simulated using pseudo stochastic sampling to determine the open and closed times of the two channel gates; the current is given according to the electrical driving force and the conductance (random number generator *ran(2)* (Press, 1988); time step 1 μsec).

B.4. MODULE 2: 3-DIMENSIONAL BUFFERED DIFFUSION OF CALCIUM

B.4.1. Overview

The second module in the numerical simulations must predict the time-dependent, 3-dimensional field of $[Ca^{2+}]$ throughout the control volume. This is a classical problem of a system of coupled, partial differential equations. The participating processes are:

[9] The time step for the numerical simulation is determined as described in section B.4.6.2.

- binding of free Ca^{2+} to unbound calcium buffers (first order kinetics)
- unbinding of Ca^{2+} from bound buffers (first order kinetics)
- diffusion of free Ca^{2+} within the control volume (Fick diffusion)
- diffusion of mobile buffers (bound and unbound) within control volume (Fick diffusion)
- (locations of hypothetical calcium channels act as sources of free Ca^{2+})

We solve the set of equations numerically (forward Euler, finite difference). This technique is one of the standard approaches to predict [Ca^{2+}] transients in nerve cells.[10] For a detailed reference, see for example Smith, 2001. Except for a very brief summary, we will not explain the technique in any detail.

One of the crucial steps in implementing the numerical approach is to determine an appropriate spatial resolution (control volume is sub-divided into cubic voxels dx^3) and a time resolution (time step dt for integrating the differential equations). Voxel size and dt critically determine the accuracy as well as the total computation time per scenario. The choice of resolution in our model is explained in detail in B.4.6. Once voxel size and dt are chosen, the numerical simulations are straight forward: During each time step, diffusion *between* voxels and buffer reactions *within* each voxel lead to a change in the concentration of each substance in each voxel. These changes must be calculated based on the concentration valid for the previous time step. Once all net changes have been calculated, all concentrations are updated to the new values, and the process starts anew. Individual equations governing the changes in concentration are described in the following sections.

B.4.2. Diffusion of calcium and other reactants

For each substance *S* and for each cubic voxel individually, the incremental change per time step in its concentration is calculated as:[11]

---

[10] Recently, Monte Carlo simulations have also become a popular tool to simulate buffered calcium diffusion (see for example Gil et al., 2000). We avoided this approach, for two reasons: (1) The additional computation time would have prevented us from testing large varieties of release site topographies within any reasonable time. (2) The simple control volume (quad) and neglecting diffusion barriers (see section B.4.2) eliminate two of the key advantages that Monte Carlo type diffusion simulations hold over the classical, differential equation approach.

[11] This formula remains valid even if neighboring voxels have a different size (see section B.4.6.1).

$$\Delta[S] = \frac{dt \cdot D}{V} \cdot \sum_{i=1}^{N} \frac{A}{d_i} \left([S]_i - [S]\right) \qquad \text{(B-1)}$$

where	*is the*
[S]	concentration of substance S in the voxel of interest, prior to the current time step
$[S]_i$	concentration of substance S in the i-th neighbor voxel, prior to the current step
dt	time step
D	diffusion coefficient of substance S in m^2 per sec; value see section B.4.4
V	volume of the voxel of interest
N	number of neighboring voxels (usually 6, except when at boundary or at border to different voxel size)
A	area of side wall of voxel of interest: dx·dx, where dx is the side length of the voxel
d_i	average of dx and dx_i, where dx is the side length of the voxel of interest and dx_i is that of the i-th neighbor voxel (in our model, voxels are cubes).

Neglecting any diffusion barriers, our model assumes free diffusion in the control volume around active zones. This is an approximation, particularly as some of the free space around active zones is in fact occupied by vesicles (as seen in Figure B-1). To validate the approximation, we analyzed the 3-dimensional reconstruction of 31 of the 600 active zones (Lübke et al., 2001). In a dome-like space around each active zone (200 nm distance from boundary of space to nearest point on active zone), there are on average 62 vesicles (not docked, i.e. not readily releasable). These vesicles occupy about 6% of the dome-space around each zone; their effect as diffusion barriers was neglected.

B.4.3. Buffering of calcium

Ca^{2+} binds to different buffer substances in the control volume. For each voxel individually, the incremental change in $[Ca^{2+}]$ per time step is calculated as:

$$\Delta[Ca^{2+}] = dt \cdot \sum_{i=1}^{N} [B_i Ca] \cdot k_{off,i} - [B_i] \cdot [Ca^{2+}] \cdot k_{on,i} \qquad \text{(B-2)}$$

where	*is the*
$[Ca^{2+}]$	concentration of free Ca^{2+} in the voxel of interest, prior to the current time step
$[B_iCa]$	concentration of the compound $Buffer_iCa$, prior to the current step
$[B_i]$	concentration of the unbound $Buffer_i$, prior to the current step
dt	time step
$k_{off,i}$	rate of calcium unbinding off the compound $Buffer_iCa$ (in per sec)
$k_{on,i}$	rate of calcium binding to $Buffer_i$ (in per Msec)
N	number of different buffer substances (up to three, in our simulations).

The incremental changes to the concentrations of the substances B_i and B_iCa are implied by the same equation.

B.4.4. Concentrations and kinetic parameters of reactants

At time zero, Ca^{2+} and buffers are at resting concentrations and at spatial equilibrium. In all scenarios, the model solution contained (*control condition*): *Calcium* at a start concentration of $[Ca^{2+}]_{rest}$= 50 nm (Helmchen et al., 1997; Table C-1), diffusion coefficient D_{Ca} = 220 $\mu m^2/sec$ (Allbritton et al, 1992); *fixed (non-diffusing) endogenous buffer* (EFB, unspecified identity) with a binding ratio of 40 (Helmchen et al., 1997), *total* concentration $[EFB]_{total}$= 80 µM, affinity k_D= 2 µM (single binding site), and a forward Ca^{2+} binding rate $k_{on} = 5 \cdot 10^8\ M^{-1}sec^{-1}$ (Klingauf and Neher, 1997; see section D.3 for sensitivity analysis); *ATP* with [ATP] = 0.58 mM, $k_{D, Ca}$ = 200 µM, $k_{on, Ca} = 5 \cdot 10^8\ M^{-1}sec^{-1}$ (Baylor and Hollingworth, 1998; with $k_{on, Ca}$ corrected for temperature; see section D.3 for sensitivity analysis), D_{ATP} = 220 um^2/sec. Kinetic parameters of ATP are for binding of ATP to Ca^{2+} only (not Mg^{2+}). The presence of 4 mM MgATP in the pipette during experiments (e.g. Borst et al., 1995) was accounted for by reducing the concentration of total ATP available for Ca^{2+} binding to 0.58 mM. The remaining ATP is assumed to stay bound to Mg^{2+} during the $[Ca^{2+}]$ transient ($k_{D, Mg}$ = 100 µM) and thus unavailable for calcium buffering (slow off rate of MgATP $k_{off, Mg}$ = 150 - 390 sec^{-1}; Baylor and Hollingworth, 1998). For some scenarios: Addition of mobile, exogenous buffers at varying concentrations: *BAPTA* ($k_{on} = 4 \cdot 10^8\ M^{-1}sec^{-1}$, k_D= 220 nM, D_{BAPTA}= 220 um^2/sec; Naraghi and Neher, 1997) and *EGTA*. The binding kinetics of *EGTA* are strongly pH-dependent. We thus used 2 sets of parameters: *"EGTA"* ($k_{on} = 10 \cdot 10^6\ M^{-1}sec^{-1}$, k_D = 70 nM; Nägerl et al., 2000) or *"slow EGTA"* ($k = 2.5 \cdot 10^6\ M^{-1}sec^{-1}$, k_D = 180 nM; Naraghi and Neher, 1997). $D_{EGTA} = D_{slow\ EGTA}$ = 220 um^2/sec.

B.4.5. Three standard approximations we avoided and why

The above approach to quantify buffered diffusion of calcium is very computationally expensive. In the past – especially with processor speeds 10 - 100 times slower than today's standards – these calculations were very time consuming. Scanning large parameter spaces and testing different hypothetical topographies was virtually impossible. Several approximations have been developed to reduce the number of computation steps. Three main ones are reviewed in detail in Neher, 1998a. Using the full, un-approximated model described above, we ran various simulations to test the validity and possible usefulness of these approximations to describe buffered calcium diffusion in the calyx of Held terminal. One of these test simulations, with parameters and single channel currents as used in chapter C, is shown in Figure B-2.

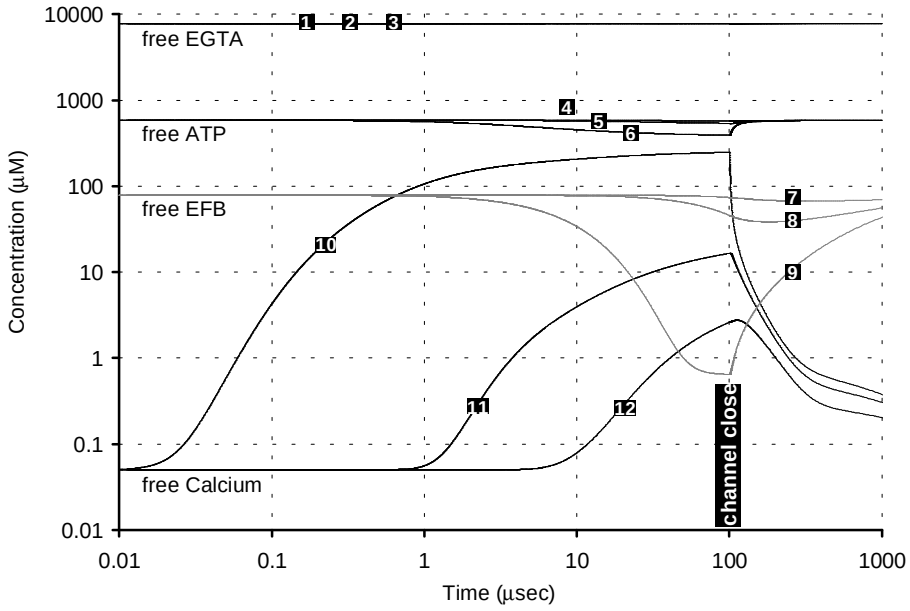

Figure B-2. Reasons not to use approximations to the full solution.
Concentrations of free (i.e. without calcium) EGTA (traces 1-3), free ATP (4-6), free endogenous fixed buffer (7-9), and free calcium (10-12) around a cluster of 12 calcium channels. All channels open at time zero, admitting a current of 0.21 pA each, and close at 100 usec. The scenario, here using 10 mM *slow EGTA*, is the same as the one described in detail in section D.4.1.1. For each substance, the plot shows the concentration vs. time at three different distances from the center of the channel cluster (= possible locations of vesicles). 1, 4, 7, and 10: at 10 nm directly above channel cluster; 2, 5, 8, and 11: at 100 nm distance from the cluster; 3, 6, 9, and 12: at 200 nm from cluster. Results show that usual approximations such as RBA, LBA, or steady state might fail to accurately describe physiological calcium signaling for release at the calyx of Held (see text).

Following is a brief description of each of the three approximations, along with the reasons why we decided *not* to use them in this work:

– *Steady state approximations of the time-dependent solutions* (Neher, 1986)

  Once a calcium channel opens, it gives rise to concentration profiles of calcium, varying in space and time. Steady state approximations assume that the buffered diffusion system equilibrates so fast, that the time prior to reaching steady state – relative to the release process the calcium controls – may be neglected. Steady state approximations thus pretend that a channel current at time t directly translates into time-invariant $[Ca^{2+}]$ profiles in space around that channel. Figure B-2 shows that this approximation is not justified for the diffusion calculations in this work. At 10 nm above a cluster of channels, $[Ca^{2+}]$ reaches nearly steady state[12] within 10 µsec of onset of a time-invariant channel

[12] Note that, in our case, this is a quasi steady state. Since our boundary conditions are either periodic or 'closed' (see section B.2.2.2), the total amount of calcium in the control volume increases upon calcium influx. This is in contrast to standard steady state approximations where calcium, after entering through discrete channels,

current. In contrast, at 100 nm and 200 nm from the channel cluster, [Ca^{2+}] does not reach steady state even after 100 µsec.[13] The time window 10 µsec to 100 µsec is crucial for the binding of calcium to the putative molecular sensor which controls the release of transmitter (Bollmann et al., 2000). Therefore, steady state approximations would not provide sufficiently accurate results.

– *Rapid buffer approximation (RBA)* (Wagner and Keizer, 1994)

  This approximation assumes that buffers' forward binding rates as well as the [Ca^{2+}] concentrations are so high that buffers 'immediately' saturate to almost 100% occupancy, thus essentially returning the buffered diffusion system to a free diffusion system. For modeling physiological calcium signals, the RBA-approximation has never been a very popular one (Neher, 1998a); physiological scenarios rarely offer conditions such that the approximation would be valid. In our case, as seen in Figure B-2, the RBA-approximation is anything but valid. Diffusiable buffers EGTA and ATP do not saturate, neither in the direct vicinity of channels, where [Ca^{2+}] is high, nor further away.

– *Linearized Buffer Approximation (LBA)* (Naraghi and Neher, 1997)

  This approximation assumes that, at any specific location around open calcium channels, the change in concentration of unbound mobile buffers is either zero or at most marginal, so that the change can be treated as a linear process, using a perturbation theory-type formalism. As expected, the slow binding buffer *slow EGTA* does not change its concentration[14] upon onset of the channel currents. Note that this does not mean that EGTA does not bind Ca^{2+}. However, the depletion of local, unbound EGTA is moderate, such that it can be replaced by diffusion of 'fresh' EGTA from regions further away from the calcium channels. In contrast to EGTA, the much faster binding buffer ATP does change in concentration, the change in concentration being largest in the direct vicinity of the calcium channels (10 nm above the channel cluster; Figure B-2). This change in concentration may be small enough to still be accurately described within the LBA equations. However, we decided not to use LBA, in order not to be limited in our choice of release site topographies and other parameters (other scenarios, with higher single

---

diffuses into free, unlimited space. However, the increase in volume average [Ca^{2+}] (50 nM to 379 nM, see section B.2.2.3 and Figure D-2 A and C) is much smaller than the local [Ca^{2+}] transients triggering release (1-100 µM). The discrepancy between quasi steady state and true steady state alone, therefore, would not have merited using the full numeric solutions instead of the much faster, steady state approximations.

[13] In this scenario, at 100 nm and 200 nm, equilibration towards steady state is especially slow due to the presence of the relatively slow buffer *slow EGTA* (10 mM) (used, for example, in the scenarios tested in section C.3.).

[14] Change is below 1%, therefore invisible in plot in Figure B-2.

channel conductance or relative locations of channels might result in more pronounced local depletion of mobile buffer).[15] More importantly, Figure B-2 shows that the non-diffussiable (i.e. non-mobile or fixed) buffer in our scenarios is strongly depleted. This is expected since, once bound to calcium, the buffer cannot be replaced by 'fresh' buffer via diffusion. In the LBA equations, fixed buffers are sometimes neglected since they do not affect the steady state profiles of $[Ca^{2+}]$ (Naraghi and Neher, 1997). As shown, however, steady state approximations would fail to accurately describe the calcium signal and its control of phasic transmitter release.

B.4.6. Three techniques to reduce the computation time anyway

The finding that standard approximations to simplify the quantification of the reaction diffusion system are not feasible in our case is rather unfortunate. Solving the full system of coupled differential equations numerically – in space and in time – is not difficult but very time consuming. Therefore, in developing the computer code to calculate buffered calcium diffusion for the calyx of Held, we employed several techniques that reduce the number of computer operations while still offering accurate results. The techniques will be explained in detail below.

B.4.6.1. I. Variable spatial resolution

The resolution required to sufficiently resolve the spatial gradients of calcium domains around single channels may be estimated from the steady state solutions of the spatial profiles: $[Ca^{2+}]$ decays with increasing distance from the channel, governed by the term (Neher, 1998a):

$$[Ca^{2+}](r) - [Ca^{2+}]_{rest} \propto \frac{1}{r} e^{(-r/\lambda)} \quad \text{and} \quad \lambda = \sqrt{\frac{D_{Ca}}{k_{on} \cdot [B_{free}]}} \qquad \text{(B-3)}$$

where	*is the*
$[Ca^{2+}]$	calcium concentration after reaching steady state
$[Ca^{2+}]_{rest}$	resting $[Ca^{2+}]$, before influx (50 nM in our scenarios)
r	distance from channel (assumed as point source in 3-dim space)
D_{Ca}	diffusion coefficient of calcium ions
k_{on}	forward binding rate of buffer
$[B_{free}]$	concentration of unbound buffer (assumes no spatial gradient, see section B.4.5).

[15] Moreover, in their discussion in Naraghi and Neher 1997, the authors conclude that the LBA formalism may not apply to $[Ca^{2+}]$ signaling at the calyx of Held.

λ evaluated for our scenarios is on the order of tens of nanometers (depending on concentration and type of buffer), implying that $[Ca^{2+}]$ decays along steep spatial gradients around an open channel, with $[Ca^{2+}]$ dropping to half their values every tens of nanometers.[16] This is shown in Figure D-3 A. Depending on the desired accuracy of the $[Ca^{2+}]$ profiles, one might conclude that a spatial resolution of voxel size = $(20\ nm)^3$ would yield sufficiently accurate results. This is true for the results of the reaction diffusion scheme, i.e. for the concentration of calcium and buffers in time and space, only. However, since the release probability (section B.5) is a supra-linear function of $[Ca^{2+}]$, an acceptable error in $[Ca^{2+}]$ of say 10% translates into $(1.1)^{3\ to\ 4}$ = 33% to 46% error in the predicted release probability.[17] We have tested the full computer algorithm at varying spatial resolutions (dx = 1-50 nm), while monitoring the errors in predicted release probability. We found that dx = 5 nm is sufficient to predict $[Ca^{2+}]$ transients and release probabilities in all scenarios tested in chapter C, yielding an accuracy of ± 0.5% (concentrations)[18] and ± 2% (release) relative to the proper results.[19]

The choice of dx has quite dramatic effects on the total computation time for each scenario. Halfing dx increases the total computation time for each scenario by a factor of about 32.[20] Fortunately, it is not necessary to use dx = 5 nm for the entire control volume. Instead, for locations away from the membrane (i.e. no release is calculated) or far away from channels,[21] spatial resolutions of dx = 20 nm yield accurate results (see above accuracy standard). Our computer program uses a scheme of variable spatial resolution in the control volume. It will be explained in detail below. As a general test to rule out any possible errors resulting from ill-chosen spatial resolution, we have regularly compared results obtained at lower

---

[16] This is not true for r→0, see footnote 18.

[17] The typical degree of supra-linearity of release vs. $[Ca^{2+}]$ is known to be about 3-4 (see section C.4.1).

[18] ± 0.5% is true for the concentrations of all buffers and in all voxels, except for $[Ca^{2+}]$ in those voxels that contain calcium channels. Since, for equation B-3, channels are considered point sources of calcium, $[Ca^{2+}]$ has a singularity at the channel itself (r→0, see equation B-3). In the numeric simulation, $[Ca^{2+}]$ in the voxel of a calcium channel will be the higher the smaller dx (this is not inconsistent with the real problem since, in reality, channels are not point sources of calcium). Note that $[Ca^{2+}]$ in the adjoining voxels will nonetheless reflect the accurate results, which are independent of dx so long as dx is small enough. Voxels containing channels were exempt from quantifying release (see section B.5).

[19] 'Proper' results were determined using dx = 1 nm. For dx→1 nm, results converge against the 'proper' results. Comparing dx = 2 nm against 1 nm, changes in the results were below 0.01%.

[20] The same control volume has 8 times more voxels. As an additional effect, the maximum time step dt decreases by a factor of 4 (see explanation in section B.4.6.2).

[21] 'Far' away from channels (hundreds of nanometers), $[Ca^{2+}]$ approaches the resting calcium concentration $[Ca^{2+}]_{rest}$ (see equation B-3), such that $[Ca^{2+}]$ is no longer proportional to $\exp(-r/\lambda)/r$.

resolution against the same scenarios at higher resolution, accepting only spatial resolutions that satisfied the above accuracy standard.

Voxel layers with different resolution: The control volume (typically 525 nm x 525 nm on membrane x 400 nm high) is subdivided into three blocks and an outer shell. Each block consists of several layers of voxels (Figure B-3). The first block typically consists of 6 layers of voxels of size $(5\ nm)^3$. (Some of the voxels in the bottom layer contain calcium channels.) The first block thus extends from the membrane (bottom) to 30 nm above the membrane. The second block extends from 30 nm to 90 nm above the membrane, consisting of 6 layers of $(10\ nm)^3$ voxels. Following are, again for a typical scenario, 8 layers of $(20\ nm)^3$ voxels. The last 60 nm (of the 400 nm height) are covered by a single shell voxel of dimensions $525 \times 525 \times 60\ nm^3$, which extends from 340 nm to 400 nm above the membrane. For periodic boundary conditions (section B.2.2.2), the shell-voxel is on top of the control volume only. For 'closed' boundary conditions, the shell-voxel extends around the four side walls of the sub-compartment, forming a shell around all three blocks of voxel layers. An advantage of the shell-voxel, in addition to further reducing the total number of voxels and thus the computation time, is that it facilitates the continuous adjustment of the total volume. This is required to accurately reflect the increase in volume average $[Ca^{2+}]$ (see section B.2.2.3).

Time-variant spatial resolution: As seen in Figure B-2, $[Ca^{2+}]$ domains collapse and spatial gradients decay within hundreds of microseconds, once calcium channels close. In our scenarios to simulate physiological conditions, spatial gradients of $[Ca^{2+}]$ have all but vanished after about 1.5 msec (Figure D-2 A). However, the simulation may not stop at this point in time as release of neurotransmitter has not yet stopped (Figure D-2 B). At 1.5 msec, to further save computation time, the computer program further reduces spatial resolution, by increasing the voxel size. Averaging the concentrations for 8 adjoining voxels each into a single, larger voxel, spatial resolution is reduced from $(5\ nm)^3$, $(10\ nm)^3$, and $(20\ nm)^3$ down to $(10\ nm)^3$, $(20\ nm)^3$, and $(40\ nm)^3$, for each block of voxels respectively. The dimension of the outer shell-voxel remains unchanged.

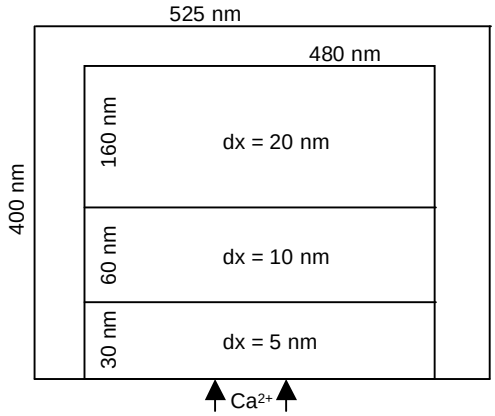

Figure B-3: Design of variable spatial resolution in sub-compartment.
Cross-section of sub-compartment. Indicated are the three blocks of three different spatial resolutions, surrounded by a shell-voxel. The spatial resolution is designed to minimize the computing time while offering sufficient resolution to accurately capture diffusion and release (see text for details).

B.4.6.2. II. Auto-adaptive time step

Calcium influx and buffered diffusion exhibit a huge range of characteristic times at which the concentrations of the participating substances change.[22] For example,[23] when a calcium channel opens and admits 0.2 pA calcium ions into a $(5\ \text{nm})^3$ voxel, $[Ca^{2+}]$ in this voxel increases from $[Ca^{2+}]_{rest} = 50$ nM by 10% within the first dt = 0.5 pS. Continuing with this time step, the simulation of 5 msec physiological time would take about 16 years.[24] As another extreme case, whenever the system operates at nearly steady state, concentration changes per time are marginal and the maximum permissible time step is given by the numeric stability requirement of the diffusion algorithm (Smith, 2001):

$$dt \leq 0.15 \cdot \frac{dx_{min}^2}{D_{max}} \qquad (B\text{-}4)$$

where	*is the*
dx^2_{min}	smallest side wall of any voxel across which diffusion of substance is modeled
D_{rmax}	maximum diffusion coefficient of all substances (220 μm^2/sec in our case).

0.15 was found by allowing larger dt and determining the threshold beyond which the numeric results turn unstable. For dx = 5 nm, the above term evaluates to 17 nsec, reducing

[22] The following argument addresses rates of change of the concentration of calcium and buffers only. Rates of change inherent in the kinetic release model – and resulting constraints on the time step – will be addressed in section B.5. In the computer program, the time step for the buffered diffusion may be decoupled from the time step for the release process.
[23] This example is taken from the step-like calcium influx scenario shown in Figure D-4.
[24] On the computer used for this work (see technical details section B.6), calculation of a single time step (diffusion, buffering, and release) takes about 50 msec (for spatial resolution dx = 5-20 nm, as described in section B.4.6.1).

the total computing time required to simulate 5 msec of physiological time to about 4 hours.[25] After 1 msec, when the spatial resolution has been reduced to dx = 10, 20, and 40 nm (see above), the maximum dt is 68 nsec. The computer code is programmed such that the simulation always operates at the maximum permissible time step dt. It monitors the *relative* changes in concentration of all substances – for each voxel individually – increasing dt gradually if changes are below the threshold (± 1%), and decreasing dt if changes exceed the threshold. This ensures that the net concentration change – in any voxel and for any substance and at any time of the simulation – never exceeds 1% per time step, while still guaranteeing that the total computing time is as short as possible.

B.4.6.3. III. Coupled diffusion of bound versus unbound buffer

For each mobile buffer participating in the reactions, the model must reflect the diffusion of two substances, the calcium-bound and the unbound buffer. In fact, the independent diffusion of bound buffer versus unbound buffer is crucial to the buffered diffusion system. It prevents, within limits, the local depletion of unbound mobile buffer (see *linearized buffer approximation*, section B.4.5). The unbound buffer acts as a sink for calcium ions, thus curtailing the spatial reach of $[Ca^{2+}]$ in the terminal (see section C.2.1). However, in order to reflect the independent diffusion of bound and unbound buffer, the model need not calculate the diffusion of both substances separately. This is explained below.

Since the diffusion coefficients of bound and unbound buffers are the same (for parameters, see section B.4.4), the equation quantifying *Fick*-diffusion (equation B-1) does not differentiate between bound buffer (CaB) or unbound buffer (B); they act – within the mathematical description – as if they were in fact the same substance. One important implication of this is that the net flux of bound and unbound buffer combined will be zero whenever there is no concentration gradient of the two substances combined. In other words, if [CaB]+[B] is the same in two adjoining voxels, CaB as well as B may diffuse, changing [CaB] and [B], but only such that [CaB]+[B] is conserved. At the start of the simulation, all substances are in spatial equilibrium; [CaB] and [B] are the same in all voxels, and thus the sum [CaB]+[B] is the same in all voxels. Once additional calcium ions enter into voxel *j*, some of the unbound buffer binds calcium so that [CaB] increases while [B] decreases. However,

[25] If dt were constant and with spatial resolution dx = 5, 10, and 20 nm throughout.

the chemical reaction leaves [CaB]+[B] unchanged. Some of the newly formed CaB will diffuse into neighboring voxels, a process crucial to and explicitly calculated by our model. Once the diffusion of CaB has been calculated, the amount of B diffusing from each neighboring voxel into voxel *j* is already known: It must be such, that [CaB]+[B] is conserved in every voxel. Therefore, the changes to [B] – for each time step and in each voxel – may be calculated by a simple sum, instead of by the more time consuming equation B-1.

In a typical scenario, the model simulates the diffusion of calcium ions as well as that of two mobile buffers, i.e. the diffusion of 5 substances (C, B_1, CaB_1, B_2, and CaB_2). Calculating the diffusion of CaB_i only – while evaluating the changes to $[B_i]$ by simple sums – reduces the total computation time per time step by about 25% (calcium influx, diffusion, buffering and release).

B.4.6.4. Summary of time saving techniques

As estimated in section B.4.6.2, simulating 5 msec worth of buffered calcium diffusion and release – for a single set of parameters – could have taken half my lifetime. With the time saving techniques described above – variable spatial resolution, auto-adaptive time step, and coupled diffusion of buffers – the time for such a simulation is reduced to about one hour. Note that this has been achieved without loss in accuracy of the final results: the $[Ca^{2+}]$ transients and release probabilities sensed by vesicles located anywhere on the membrane. One hour is a feasible time to scan large parameter spaces of exogenous buffer concentrations and of hypothetical locations of calcium channels and vesicles. The results presented in chapter C of this thesis, the topography of release sites, would not have been possible without a fast, yet accurate computer model.

B.5. MODULE 3: RELEASE OF NEURO TRANSMITTER

B.5.1. Overview

To quantify release triggered by $[Ca^{2+}]$ transients, our model uses, alternately, two release models, termed Release Model A (Bollmann et al., 2000) and Release Model B (Schneggenburger and Neher, 2000). Both models and their parameters are calibrated to describe phasic transmitter release at the calyx of Held.[26] The models are from independent

[26] As it is not the objective of this study to explain, verify or further discuss the release models, we will not describe them in detail. For details on the models, as well the parameters calibrated for the calyx of Held, the

experimental studies. They describe the putative, calcium-sensitive release sensor by different, multiple-state kinetic models and ascribe different calcium sensitivities to each releasable vesicle (Figure C-3 B). We deliberately use both models – in order to demonstrate the impact on predicted [Ca^{2+}] transients as well as the robustness of our findings regarding the topography of release sites (chapter C and discussion in section E.1).

The release models quantify the probability that a particular, individual vesicle will release its neurotransmitter in response to an action potential. We term this probability $RP_{vesicle}$ (section B.5.2). Comparison of predicted $RP_{vesicle}$ to experimental data is not possible because, at the calyx of Held, the release probability of individual vesicles cannot be measured. The released neurotransmitter, whose action is recorded postsynaptically, is comprised of the contribution of typically 200 of the 800-2000 readily releasable vesicles, distributed over the circa 600 active zones at the presynaptic membrane (Table C-1). Experiments at the calyx of Held only determine the average $RP_{vesicle}$ across all readily releasable vesicles. Therefore, in order to compare predictions of the model to experimental data, the model must also quantify the average $RP_{vesicle}$ of all vesicles in the terminal. We term this probability $RP_{terminal}$.

Employing actual release models, with a defined sensitivity to calcium concentrations as well as a defined saturation level,[27] means a significant advance in modeling physiological calcium signaling. Previously, release triggered by different, hypothetical calcium transients could be evaluated in relative terms only (e.g. [Ca^{2+}] = 20 µM instead of 10 µM means about 8 times more release).[28] For the first time at a central synapse, it is possible to quantify, for any hypothetical calcium transient, the resulting release probability in absolute terms. This is crucial to our results on release site topography.

Depending on the assumed topography, vesicles in our model may be placed at different locations relative to the calcium channels, thus sensing different [Ca^{2+}] transients, which in turn result in different $RP_{vesicle}$. Since the release models are highly supra-linear, considering average [Ca^{2+}] transients does not predict average $RP_{vesicle}$. Appreciating the fact that $RP_{terminal}$

---

reader is referred to Bollmann et al., 2000 (Release Model A) and Schneggenburger and Neher, 2000 (Release Model B).

[27] I.e. the [Ca^{2+}] for which a further increase in [Ca^{2+}] does not mean a further increase in the predicted release probability.

[28] The typical degree of supra-linearity of release vs. [Ca^{2+}] is known to be about 3-4 (see section C.4.1).

measured in experiments may be comprised of a multitude of different $RP_{vesicle}$ – triggered by a multitude of different $[Ca^{2+}]$ transients – is a novel and pivotal aspect of this work. It results in a series of new findings on the topography of release sites (chapter C); and it provides the synapse with crucial advantages for its physiological function (section D.4.2).

B.5.2. Calculating $RP_{vesicle}$ and $RP_{terminal}$

A kinetic release model is described by a mathematical function F that translates any time-dependent concentration $[Ca^{2+}](t)$ into a time-dependent release probability $RP_{vesicle}(t)$. $RP_{vesicle}(t)$ is the cumulative release probability at time t, i.e. the probability that a vesicle that has been subjected to $[Ca^{2+}](t)$ between time zero and time t releases its neurotransmitter *at any time* between time zero and time t. The process of release itself is considered a stochastic all-or-nothing event, which happens instantaneously at any time between zero and t.

$$RP_{vesicle}(t) = F_{Release\ model}\left([Ca^{2+}](0...t)\right) \qquad (B\text{-}5)$$

where	*is the*
$[Ca^{2+}](t)$	time-dependent concentration of Ca^{2+} *at the very location* where the molecular release sensor is presumably located[29]
$F_{Release\ model}$	set of coupled differential equations, describing the binding and unbinding of calcium to a set of receptors which, upon binding of multiple receptors simultaneously, trigger the release/fusion of the vesicle (see Bollmann et al., 2000; Schneggenburger and Neher, 2000).

Our model solves F, a set of coupled differential equations, numerically (forward Euler, finite difference), with a time step dt such that the relative change from one kinetic state to another never exceeds ±1% per time step. We assume that release of individual events is independent, and that the binding of Ca^{2+} to the release sensor does not affect local $[Ca^{2+}]$ (Yamada and Zucker, 1992). $RP_{terminal}(t)$, at any time t, is the (arithmetic) mean of $RP_{vesicle}(t)$ across all vesicles.

B.5.3. $RP_{terminal}$ of 600 active zones simulated within a single sub-compartment

One of the key features of our model is that vesicles at the about 600 active zones of a single terminal may have different locations relative to the release controlling calcium channels.

---

[29] Our model does not differentiate between the location of a vesicle and the presumed location of the molecular release sensor (which might in fact consist of several molecules). To calculate $RP_{vesicle}$ for a vesicle located, for example, at "80 nm from a calcium channel", we evaluate F for the $[Ca^{2+}](t)$ in the voxel 80 nm away from the channel (first voxel layer at membrane). Note that the vesicles themselves have a diameter of about 50 nm (Figure B-1). It is not known where the molecular release sensors are located with respect to the vesicles; however, it is usually assumed that they are located in-between the vesicle and the presynaptic membrane (Matthews, 2000).

Since $RP_{vesicle}$ is a non-linear function of $[Ca^{2+}]$, $RP_{vesicle}$ for each location must be explicitly modeled; considering only average locations yields misleading results (see for example section C.2.3). Fortunately, explicitly modeling different locations of vesicles across different active zones may be achieved without simulating buffered calcium diffusion for all 600 active zones individually. Instead, we simulate $[Ca^{2+}]$ transients around only one active zone, while evaluating $RP_{vesicle}$ for a multitude of different locations relative to the release controlling calcium channels at the one active zone. The average of $RP_{vesicle}$ across all presumed locations (= $RP_{terminal}$) thus represents the average release probability of all readily releasable vesicles located, in reality, at different active zones of the same terminal.

Calculating $[Ca^{2+}]$ dynamics and $RP_{terminal}$ at only one active zone in lieu of all 600 active zones makes the following simplifying assumptions: (1) The number of calcium channels, as well as their position relative to each other, are the same at each active zone.[30] Only the position of vesicles relative to these channels varies across active zones. (2) The effect of vesicles on $[Ca^{2+}]$, as diffusion barriers, is marginal such that the spatial profile of $[Ca^{2+}]$ around calcium channels is the same at each active zone.[31] Note, however, that our model does not assume that $[Ca^{2+}]$ dynamics themselves are the same at each active zone. This is explained below.

B.5.3.1. Accounting for stochastic channel opening

The above approach is especially time efficient for calculating $RP_{terminal}$ when assuming the same, average calcium current for each channel. For such scenarios, the model predicts $RP_{terminal}$ in a single run of buffered calcium diffusion and release in the control volume. However, in reality calcium currents of individual channels are stochastic. This means that, even though the relative location of calcium channels are considered the same at all active zones, spatial patterns and time course of calcium influx – and thus spatial profiles of $[Ca^{2+}]$ transients – vary from active zone to active zone. As a result, two vesicles presumed at the same location relative to calcium channels may still sense different $[Ca^{2+}]$ transients if they are located at different active zones. To account for effects of stochastic single channel

[30] Or rather: Any variations in number or relative position are such that they do not affect $RP_{terminal}$ such that it would change our findings on release site topography. With regard to the discussion in section E.2.2, a possible variation in the number of calcium channels across active zones represents a possible, *additional* source of heterogeneity which we cannot rule out.

[31] See quantification of occupied volume in section B.4.2.

currents, the model simulates calcium dynamics and resulting $RP_{terminal}$ many times,[32] each time using different, stochastically varied channel currents (see Hodgkin-Huxley model, section B.3.). For such cases, we report Mean ($RP_{terminal}$) ± SEM. Accounting for effects of stochastically varying [Ca^{2+}] transients, instead of considering only average [Ca^{2+}], offers crucial insights into the topography of release sites and into its functional relevance (results in section C.4; discussion in section E.3.2).

B.5.3.2. Distribution function for vesicle distances

As explained in detail in chapter C, the various release site topographies tested in this work each imply a characteristic distribution of vesicle locations. For simple distributions – such as: vesicles are located anywhere on a circular patch around a cluster of calcium channels – the model simply calculates $RP_{vesicle}$ for all locations on the patch. For such cases, $RP_{terminal}$ is equal to the average $RP_{vesicle}$ across all locations. For more complex topographies, such as the cluster topography introduced in section D.1, the model evaluates $RP_{vesicle}$ for the full range of distances *D* from the channel cluster. In a second step, it calculates $RP_{terminal}$ by weighting $RP_{vesicle}(D)$ with the distance distribution function w(*D*) implied by the topography:[33]

$$RP_{terminal} = \sum_{i=1}^{N} RP_{vesicle}(D_i) \cdot w(D_i) \qquad (B\text{-}6)$$

where	*is the*
N	total number of distances (resolution 5 nm) at which vesicles may be located
D_i	distance i
$RP_{veside}(D_i)$	RP_{veside}, evaluated in the voxel located at distance D_i from the cluster of calcium channels
$w(D_i)$	probability that, at any active zone, a vesicle is located at distance D_i from the calcium channels (Σ w(D) = 1).

B.5.4. Comparing predicted release with measured release: $RP_{terminal}$, release rate and EPSC

As has become apparent in this chapter, predicting $RP_{terminal}$ for the calyx of Held via numerical simulations is not easy. However, 'measuring' $RP_{terminal}$ in electrophysiological experiments is probably harder still.[34] Since comparing predicted to measured release forms the basis of the results presented in this work, this section explains which experimental measure for 'release' we chose for this study and why.

---

[32] Typically around hundreds of times to yield SEM of about 1% of the converged $RP_{terminal}$.
[33] w(D) implied by the cluster topography used in chapter D is shown in Figure D-1.
[34] Having done it myself, I do know what I'm talking about.

For fast synapses such as the calyx of Held, the time course of $RP_{terminal}$ cannot be measured directly. All experimental data on release used in this work is based on *indirect* quantification of the amount of transmitter released from presynaptic vesicles. Recording the post-synaptic currents that are evoked by the neuro-transmitter (*excitatory post-synaptic currents* or EPSCs), it is possible to quantify the number of vesicles released in response to an action potential.[35] Dividing this number by the total number of releasable vesicles, also accessible in experiments, yields $RP_{terminal}$ (see references in Table C-1). While the model predicts the full time course $RP_{terminal}(t)$, experimental data only offers safe estimates for the *total* number of vesicles released in response to an action potential. This corresponds to $RP_{terminal}(t = 5\ msec)$ in our model, a time beyond which predicted $RP_{terminal}$ no longer increases. While techniques have been developed to extract the full time course of $RP_{terminal}(t)$ from that of the measured EPSC, such 'deconvolutions' involve a number of parameters, and the implied $RP_{terminal}(t)$ can only be estimated (Sakaba and Neher, 2001b and reference therein). To evaluate our model's results by comparing predicted with measured release, we therefore focus on $RP_{terminal}$ ($t = 5$ msec) only.

Merely for illustrative purposes, our model calculates the *release rate(t)* of the terminal. Evaluating $dRP_{terminal}/dt$ times the total number of readily releasable vesicles in the terminal,[36] the release rate quantifies the absolute rate at which vesicles fuse with the membrane at any time t during synaptic transmission (Figure D-2 B and D). The release rate may be translated into a predicted EPSC (see above comment for difficulties). The EPSCs we show were calculated by convoluting the terminal release rate with a so called miniature EPSC, as described in Bollmann et al., 2000 (Figure D-5).

B.6. SOME DETAILS ON THE COMPUTER PROGRAM

The complete algorithm described in the above sections was implemented in Ansi C code. The program ran on a multiprocessor computer, so that several parameter scenarios could be simulated at the same time (*Silicon Graphics Oregon 2000*; MIPS RP1200 processors with

---

[35] This study, as well as the Release Models A and B, concentrate on the so called fast or *phasic* component of release, which can be estimated from the amplitude of the post-synaptic EPSC. Other, so called *delayed* release is not covered by our model; the experimental data listed in Table C-2, used to evaluate the model's results, regards only phasic release.

[36] Number of readily releasable vesicles = 800 for Release Model A, 2000 for Release Model B (see Table C-1).

300 MHz).[37] We ensured the correctness of the reaction-diffusion algorithm by comparing the [Ca^{2+}] spatial profiles to analytical solutions for the steady state profiles (Neher, 1998a). In addition, the program monitors the total amounts of all reactants in the control volume. In the course of long simulations involving 100 000 and more time steps, numeric errors did accumulate such that the total amount of calcium deviated by as much as 10% from the correct amount. We therefore increased the numeric accuracy from 8-digit floating point to 16-digit floating point. This reduced relative changes in total amounts to less than 10^{-6}, even for simulations involving hundreds of thousands of time steps.

[37] A parallel version of the code has been developed as well. Thank you to Babak Hadj-Hosseini.

C. RESULTS ON LIKELY RELEASE SITE TOPOGRAPHY

C.1. INFERRING CONSTRAINTS ON RELEASE SITE TOPOGRAPHY - METHODOLOGY

Our findings on the functional and spatial organization of vesicles and calcium channels at release sites of the calyx of Held (*topography of release sites*) are based on the quantitative model described in chapter B. Release probabilities (RP) predicted by the model are compared against RP measured in experiments, under a variety of experimental conditions. Systematic comparisons, scanning large parameter spaces, allowed us to infer three distinct characteristics on the topography of release sites likely to be found at the calyx of Held. The methodology of inference will be explained below.

The model calculates buffered calcium diffusion and phasic transmitter release, simulating a single, typical calyx of Held terminal at the developmental stage postnatal day 8-10. The experimental data in Table C-1 directly determine crucial parameters of the virtual terminal in which the simulations are carried out: volume, membrane surface area, size of active zones, whole cell [Ca^{2+}] during single action potentials, and the endogenous calcium buffer capacity.[38] To quantify release in response to any simulated [Ca^{2+}] transient, the model uses, alternately, two release models for the calyx of Held, termed Release Model A (Bollmann et al. 2000) and Release Model B (Schneggenburger and Neher, 2000). The only remaining crucial, but unknown property is the topography of release sites: the number and location of calcium channels in the presynaptic membrane (unknown for the calyx of Held), particularly their location relative to the readily releasable vesicles at active zones (see chapter E for sensitivity of other parameters). Although the conductance of single calcium channels at the calyx of Held is unknown as well, its value in the model is constrained such that the particular hypothesized topography yields a predicted release probability (RP) as observed in experiments. We define RP as the fraction of all readily releasable vesicles that are released during a single action potential (phasic release only).

Calyx of Held terminals (of the same animal) vary with respect to the properties listed in Table C-1 (Morest, 1968; Forsythe, 1994). Although combining results from different studies, the properties of the model terminal are internally consistent, and thus likely to be found in a real, single terminal (e.g. not above average whole cell calcium current combined with below

[38] *Buffer capacity* is defined as the total number of calcium ions entering the terminal during a single action potential, divided by the number of calcium ions entering *and* remaining free, i.e. un-buffered (see also part B).

average increase in [Ca^{2+}]). While the model does not simulate variability across terminals, the variability of phasic release within a single terminal (from release site to release site) is explicitly simulated.

Table C-1. Experimental data used to set properties of virtual/model terminal

Terminal volume[a]	400 um^3	(Lübke et al., 2001; Helmchen et al. 1997)
Terminal membrane surface[a]	2000 um^2	(Lübke et al., 2001)
Terminal *height*[b]	400 nm	(Lübke et al., 2001)
% of terminal surface identified as Active Zones (= release sites)	2%	(Lübke et al., 2001)
Number of active zones[c]	600	(Lübke et al., 2001)
Diffusional separation of any Active Zone to its nearest neighbor	200 nm - 1000 nm median: 400 nm	(Lübke et al., 2001);
Size of active zones (approx. as circular patches of varying radii)[d]	0.052 ± 0.024 um^2 (s.d.) (mean radius = 125 nm)	(Lübke et al., 2001; also see Rowland et al., 2000);
Total Ca^{2+} influx during single, physiological action potential	0.93 pC = 12 µM in 400 um^3	(Helmchen et al., 1997)
Endogenous Ca^{2+} binding ratio	40 (2.5% of ions remain free)	(Helmchen et al., 1997)
Δ[Ca^{2+}] during single action potential[e]	from 50 nM (resting) to 379 nM	(Helmchen et al., 1997); see Figure D-3 A and C
Whole cell I_{Ca}	peak: 2.41 nA, half width (fwhm) 383 µsec	(Borst and Sakmann, 1998); see Figure C-3 A for time course
Ca^{2+} channel open probability during physiological AP[f]	69%	(Borst, Sakmann, 1998)
Calcium sensitivity of release[g]	5-site co-op: Model B 5-site indep.: Model A	(Schneggenburger and Neher, 2000) (Bollmann et al., 2000); see Figure C-3 B
$RP_{terminal}$ of un-patched terminal[h] ($[Ca^{2+}]_{ex}$ = 2 mM)	Model B: 10% (of 2000) Model A: 25% (of 800)	(Schneggenburger and Neher, 2000) (Bollmann et al., 2000)

(a) Parameters taken from the EM study of calyx of Held (rat) are averages of minimal and maximal values reported in Lübke et al., 2001. (b) Average distance between membrane facing the cleft and that opposite the cleft; consider terminal as a thin disk with surface 1000 um^2 at top/bottom, height ~ 400 nm, and volume 400 um^3. (c) Corresponding to an average of 1.3 (Release Model A) or 3.3 (Release Model B) readily releasable vesicles docked per active zone. (d) The value is smaller than 0.073 um^2 reported in Lübke et al., 2001. 0.073 um^2 includes uneven surface of the Active Zones which does not contribute to diffusional distance (author's independent analysis of the EM-contour data provided in Lübke et al., 2001. (e) 379 nM is the equilibrium of [Ca^{2+}] after adding 12 µM free Ca^{2+} to the terminal (with ATP and endogenous buffer). (f) As predicted by a 2-gate Hodgkin Huxley Model fitted for the calyx of Held (g) All conclusions presented in this paper were tested with two release models measured for the calyx of Held: a kinetic release model with 5 co-operative (sequential) binding sites (termed Release Model B) and one with 5 independent binding sites (Release Model A). The number of quanta released during physiological action potentials, $RP_{terminal}$·RRP (Readily Releasable Pool) was the same in both studies (~ 200). Figure C-3 B shows a direct comparison of the models' calcium sensitivities. (h) $RP_{terminal}$ = release probability during single action potential: defined throughout this paper as the total number of vesicles (as fraction of the readily releasable pool) that are released in response to a single action potential (phasic release only).

As will be shown, properties in Table C-1 alone (release under physiological conditions) do not serve to discriminate between likely/unlikely release site topographies. Therefore, we also considered non-physiological conditions affecting release (Table C-2): exogenous calcium buffers (dose-dependent), lowered $[Ca^{2+}]_{ex}$ in the extra-cellular solution, and reduced open probability of Ca^{2+} channels. The model explicitly simulates these conditions and their predicted effect on RP. The effect on RP critically depends on the channel-vesicle topography assumed in the model. Comparing the results of the model to respective experimental data thus allowed us to ascertain whether a particular, hypothesized topography is likely to be present at the real terminal or not.

Table C-2. Experimental data used to discriminate between topographies

$RP_{terminal}$ of terminal dialyzed with exogenous buffers[a]	EGTA: 0.2 mM 25 % 1 mM 15.1 ± 1.3% (SEM) 10 mM 12.6 ± 1.8%	(Borst and Sakmann, 1996)
	BAPTA: 0.05 mM 25 % 1 mM 8.8 ± 1.3% 10 mM < 1%[d]	(Borst et al., 1995) Model results: Figure D-3 B
Apparent Hill Coeff.: $RP_{term} \propto \left(\int I_{Ca} \cdot dt\right)^n$, when reducing $[Ca^{2+}]_{ex}$[b]	n = 2.2 - 4	(Wu et al. 1999; Barnes-Davies and Forsythe, 1995; Borst and Sakmann, 1999a); Model results: Figure C-3 D
$RP_{term} \propto \left(\int I_{Ca} \cdot dt\right)^m$, when reducing channel open prob. by AP waveforms[c]	m = 3 - 3.5	(Borst and Sakmann, 1999a) Model results: Figure C-3 C
$RP_{term} \propto \left(\int I_{Ca} \cdot dt\right)^m$, when partially blocking P/Q-type calcium channels[c]	m = 3.7±0.2 (SEM)	(Wu et al. 1999)
$RP_{term} \propto \left(\int I_{Ca} \cdot dt\right)^m$, when partially blocking N- and R-type calcium channels	m = 1.4±0.1 (SEM)	(Wu et al. 1999)

(a) In the referenced studies, terminals dialyzed with little exogenous buffer (0.2 mM EGTA or 0.05 mM BAPTA) had the same $RP_{terminal}$ as prior to patching (control). $RP_{terminal}$ given here are for the Release Model A (control = 25%). For the Release Model B, scale $RP_{terminal}$ under buffers accordingly (control = 10%). (b) Note that instead of $RP_{terminal}$ (see Table C-1), experimental studies usually use EPSC amplitude as a measure for release. For the fast, phasic component of action potential evoked release $EPSC_{peak} \propto RP_{terminal}$. Some studies report n for release vs. $[Ca^{2+}]_{ex}$ (for either varying or adjusted $[Mg^{2+}]_{ex}$), or vs. $I_{Ca,\,peak}$. However, $\int I_{Ca} \cdot dt \propto I_{Ca,\,peak} \propto [Ca^{2+}]_{ex}$, when reduced from 2 mM to 0.25 mM (Borst and Sakmann, 1996, Helmchen et al., 1997). (c) The nomenclature of n and m, which measure calcium co-operativity and/or channel co-operativity, follows that in Wu et al. 1999 (n = 2.7). See section C.4 for additional explanation. (d) Implied phasic release probability during action potentials as estimated from Borst and Sakmann, 1999b.

We present three main conclusions on the topography of release sites (conclusions I - III). The conclusions yield three independent constraints on how calcium channels and vesicles may be spatially organized in order to comply with the experimental data. Each conclusion is based on different aspects of the experimental data, and each regards different aspects of the

topography of release sites. Conclusion I regards the location of vesicles at different release sites of the same terminal. Conclusion II regards the density and relative location of calcium channels in the presynaptic membrane. Conclusion III regards how many calcium channels control the release of a single vesicle. In conclusion IV, the constraints given in I-III are merged into a full topography – the relative location of both Ca^{2+} channels and vesicles at individual release sites.

C.2. CONCLUSION I: THE DISTANCE BETWEEN A VESICLE AND ITS RELEASE CONTROLLING CHANNEL(S) VARIES ACROSS RELEASE SITES

At the calyx of Held synapse, the distance between a vesicle and the calcium channel(s) controlling its release is not known. Knowing the calcium sensitivity of the release controlling molecular sensor does not solve this problem, the reason being that the single channel conductance is not known. The $[Ca^{2+}]$ transient required to release a vesicle could be provided by a channel at distance d and with conductance c, or, alternatively, by a channel twice as far away but with about twice the conductance (see below). As will be shown, this scaling behavior would prevent us from inferring at what distances vesicles are likely to be located at the release sites. However, the scaling is broken when experimental data on exogenous calcium buffers are considered.

C.2.1. Exogenuous buffers

When a calyx of Held terminal is dialyzed with exogenous calcium buffers such as EGTA or BAPTA, phasic release is reduced in a concentration dependent manner. 10 mM EGTA reduces RP to about 0.5 of control (unpatched terminal); 1 mM BAPTA, which binds Ca^{2+} much faster than EGTA, reduces RP to about 0.35 of control (Borst and Sakmann, 1996; Borst et al., 1995; Table C-2). The release suppressing effect of mobile buffers is generally ascribed to their effect on $[Ca^{2+}]$ transients. EGTA and BAPTA intercept part of the Ca^{2+} diffusing from the channels to vesicles, thereby reducing the $[Ca^{2+}]$ transients reaching the vesicles. The theoretical background of such reaction diffusion of calcium and buffers is described in Neher, 1998a. In combination with experimental results, diffusion calculations may be used to infer characteristic distances between release controlling channels and vesicles. This has been addressed previously for the calyx of Held (Naraghi and Neher, 1997). Here, we confirm the earlier result, while offering a different interpretation.

C.2.2. Single domain scenario

We start by assuming that every vesicle at an active zone in the terminal is located at some fixed distance from a single calcium channel that controls its release. Figure C-1 B shows the release probability of a single vesicle ($RP_{vesicle}$) as a function of this distance. In the simulations, the time course used for each channel's I_{Ca} was equal to that of the whole cell I_{Ca} measured in experiments (Figure C-3 A). I_{Ca} gives rise to a $[Ca^{2+}]$ transient whose peak amplitude decays rapidly with increasing distance from the channel. Therefore, we increased the single channel conductance for increasing distances (Figure C-1 A, right axis) such that $RP_{vesicle}$ remained at 25% for the control condition (control = endogenous fixed buffer and ATP only). In contrast to the control condition, the predicted $RP_{vesicle}$ under addition of exogenous buffers was strongly dependent on distance. This is expected since, in a single domain scenario (Neher, 1998a), the reduction in $[Ca^{2+}]$ relative to $[Ca^{2+}]$ under control is the stronger, the further away from the channel the vesicle is located (Figure C-1 A). (Figure C-1 A and B show results using Release Model A; analogous calculations using Release Model B yielded the same conclusion, not shown.) In comparing the differential effect of exogenous buffers EGTA and BAPTA at any one distance, Figure C-1 B confirms a result reported previously (Naraghi and Neher, 1997). There is no distance at which predicted release is consistent with experimental results for both EGTA and BAPTA. For any distance at which the predicted suppression of $RP_{vesicle}$ by 10 mM EGTA is comparable to that observed in experiments (25 - 40 nm, dashed box in Figure C-1 B), the predicted suppression of 1 mM BAPTA is much stronger than that in experiments. Note that, at much larger distance (several hundred nanometers), local $[Ca^{2+}]_{local}$ approaches the volume average $[Ca^{2+}]_{vol}$. At such large distance, $[Ca^{2+}]_{local}$ in the presence of 10 mM EGTA is actually lower than that in the presence of 1 mM BAPTA (dissociation constant $k_{D, EGTA} \sim k_{D, BAPTA}$). However, imaging studies show that $[Ca^{2+}]_{vol}$, during single action potentials, stays below 1 μM, a concentration too low to trigger phasic transmitter release (Schneggenburger and Neher, 2000; Bollmann et al., 2000).

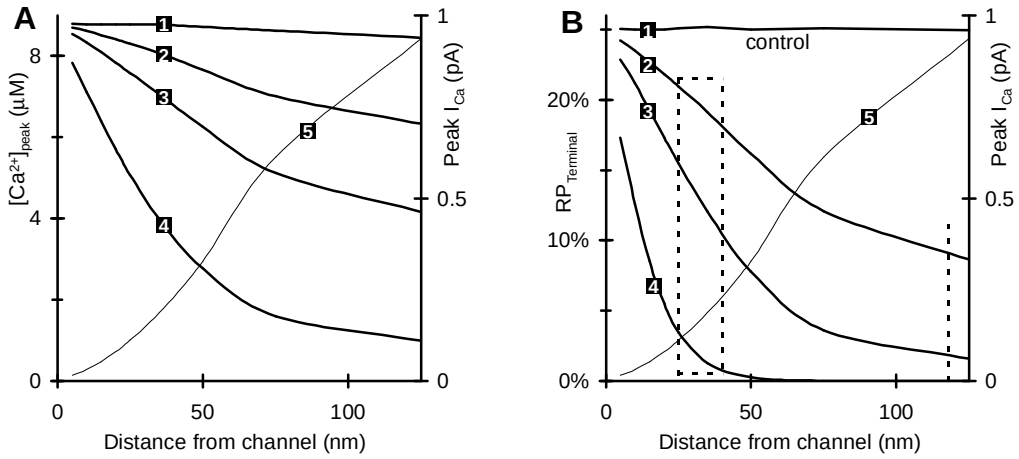

Figure C-1. Effect of vesicle location on release probability.

(A) Predicted peak [Ca^{2+}] if all vesicles *were* located at the same distance from the channel/cluster that controls their release (Release Model A). Traces 1-4 represent 4 different buffer conditions. 1: endogenous fixed buffer (EFB) and ATP (= control condition). 2: EFB, ATP, and 10 mM *slow EGTA*. 3: EFB, ATP, and 10 mM Egta. 4: EFB, ATP, and 1 mM BAPTA. 5: peak current per channel/cluster required to achieve release probability ($RP_{vesicle}$) of 25% for the control condition (right axis). (B) Predicted average $RP_{vesicle}$ ($RP_{terminal}$) for the same scenarios. Traces 1-4 for buffer conditions as in (A). Trace 5 same as in (A). Dashed box indicates distance where release under EGTA, but not BAPTA, is similar to experiment. Vertical dashed line indicates *average* vesicle distance 118 nm of the cluster topography used in chapter D. Results suggest that vesicles are located at non-uniform distance from release controlling channels (conclusion I).

C.2.3. Novel interpretation of single domain calculations

The results shown in Figure C-1 B assumed that a vesicle is controlled by a single channel. However, the above dilemma is not resolved by concluding that vesicles are controlled by multiple channels instead of only one. Replacing the single channel in the above calculation with n channels – all at the same distance to the vesicle but with conductance reduced to 1/n – would give similar results. (As expected from the channel currents <1 pA, mobile buffers did not saturate during any of the scenarios shown in Figure C-1. Thus, the [Ca^{2+}] domains of single channels contribute linearly (Neher, 1998a).) Another assumption implicit in the analysis is more crucial: In comparing $RP_{vesicle}$ in Figure C-1 B to experimental results – which measure the average release probability across all vesicles in the terminal – we have implicitly assumed that all readily releasable vesicles in the terminal are located at the same distance from their release controlling channel. Under this assumption, the experimental observation could not be explained. We therefore conclude that the distance of individual vesicles to their release controlling Ca^{2+} channel(s) is likely to vary. In fact, this is suggested by the experiments themselves: While some vesicles seem to be located sufficiently far from calcium channels to be affected by kinetically slow EGTA (10 mM), other vesicles, in the same terminal, could be located closer to channels so that kinetically fast BAPTA (1 mM)

suppresses their release only moderately. To test this quantitatively, we assumed the following, simplified distribution of distances: Every active zone is a circle with radius = 125 nm (see EM-Data Table C-1). Every active zone has only one calcium channel controlling release. The channel is located at the center of each active zone. Vesicles are located at random anywhere on the active zones, with a distance ranging between 0 and 125 nm from the center, average distance 83 nm. With $I_{Ca,\,peak}$ = 0.66 pA per channel, the average $RP_{vesicle}$ across all vesicles was 33.5% for the control condition, 19.6% when adding 10 mM EGTA, and 9.5% when adding 1 mM BAPTA (Release Model A). Even for this simplified distribution, predicted average $RP_{vesicle}$ are similar to RP observed in experiments. The quantitative mechanism that favors heterogeneous location of vesicles in reproducing experimental data will be illustrated in detail in chapter D.

C.3. CONCLUSION II: RELEASE-RELEVANT CALCIUM SOURCES ARE SEPARATED BY DISTANCES > 250 NM

Having addressed the distance between calcium channels and vesicles, we now focus on the distance between calcium channels themselves. Since we know the peak whole cell calcium current per action potential ($I_{Ca,\,peak}$ = 2.4 nA) as well as the membrane area for the terminal (2000 μm^2), we can estimate the calcium current per membrane area during phasic transmitter release at the calyx of Held to be on the order of 1 $pA\mu m^{-2}$. However, since the single channel conductance is not known, we do not know how many channels in the membrane contribute to the total I_{Ca}, and thus cannot estimate an average distance between calcium channels. Moreover, the density of calcium channels at active zones may differ from the average density of the terminal.

C.3.1. Multiple domain scenario

We will now show how the experimental findings on the effects of exogenous buffers may be used to infer a minimum distance of Ca^{2+} channels that control phasic release. In simulations, channels were arranged on a regular grid, covering the membrane. The separation of neighboring channels (grid constant *d*) as well as the single channel conductance was varied for different scenarios. The time course used for each channel's I_{Ca} was equal to that of whole cell I_{Ca} (Figure C-3 A).

C.3.2. Example with grid constant 60 nm

Using as an example $d = 60$ nm, Figure C-2 A illustrates how domains from individual channels in a regular grid combine into a total [Ca^{2+}] signal (left axis); how this signal is modified in the presence of exogenous buffers; and how this affects the predicted release probability of vesicles at different, hypothetical locations in the grid (right axis). For $d = 60$ nm, there is no location, at which the $RP_{vesicle}$ under 1 mM BAPTA is similar to 0.35 of that under control conditions. In the direct vicinity of a channel, the peak of the [Ca^{2+}] transient under 1 mM BAPTA is about half of control. At that location, however, $RP_{vesicle}$ (2.6%) is only 0.05 of control (52%). For all other locations, the release suppressing effect of 1 mM BAPTA relative to control is even stronger. This means that there is no possible distribution of vesicles within the $d = 60$ nm grid that would be in agreement with experimentally observed phasic release probabilities (vesicles at fixed distance to next channel, random location, or any other distribution).

C.3.3. Scanning parameter space of grid constant

Extending the analysis, we calculated scenarios for d ranging between 5 nm (~ uniform influx through membrane) and 500 nm. This corresponds to between 40 million and 4000 channels on the ~ 1000 μm^2 membrane facing the cleft. For d = 5 nm, $I_{Ca,\ peak}$ = 0.00015 pA per channel would be needed to yield $RP_{vesicle}$ = 25% (using Release Model A; 0.00033 pA when using Release Model B; Figure C-2 C and D). While keeping the total Ca^{2+} influx into the terminal constant, we increased d (and the current per channel as d^2), thus increasing diffusion distances for Ca^{2+} between channels. This leaves the peak of the average [Ca^{2+}] transient (average across all locations in the grid) nearly constant (8-9 µM for control, 4.5-4.9 µM for 10 mM EGTA, 1.9-2.2 µM for 1 mM BAPTA). However, the spatial profile of [Ca^{2+}] transients becomes more and more heterogeneous, leading to a steeper gradient between the peaks of [Ca^{2+}] in the direct vicinity of channels and the troughs between surrounding channels. For d = 480 nm, the peak of the predicted [Ca^{2+}] transient in the direct vicinity of channels is 350 µM, the peak of the average transient is 9.0 µM, and the peak at distance $d/2$ from two neighboring channels is 4.1 µM (Figure C-2 B). Similar to the analysis for conclusion I, we again started by investigating whether there is any hypothetical location in the grid of channels (i.e. all vesicles located at *same* distance from nearest channel), for which the predicted $RP_{vesicle}$ is in agreement with exogenous buffer experiments. At $d = 5$ nm, the peak of the [Ca^{2+}] transient under 1 mM BAPTA (1.94 µM) is 0.24 of that of control. $RP_{vesicle}$

(= 0.06%) is only 0.0024 of control, i.e. more than a hundred times less than that observed in experiments (implying a supra-linearity of n = 4.2 when expressing $RP_{vesicle} \propto [Ca^{2+}]^n_{peak}$). As seen in Figure C-2 A and B, the ratio of $[Ca^{2+}]_{peak}$ under control vs. $[Ca^{2+}]_{peak}$ under exogenous buffers is the larger, the further the location from any one channel, and the larger d. For example, if vesicles and channels were co-localized – in a grid of d = 200 nm – then $[Ca^{2+}]_{peak}$ under 1 mM BAPTA would be 0.75 of $[Ca^{2+}]_{peak}$ under control conditions, and RP_{BAPTA} would be approximately $0.75^4 \cdot RP_{control}$, i.e. about 32% of RP under control conditions (in agreement with experiments). However, the predicted RP under 10 mM EGTA for this scenario would be too high (RP 0.7 of control). We found that there is no location within a grid (for any d), at which the predicted effects of BAPTA and EGTA are both in agreement with experiments. As in conclusion I, this changes when considering a distribution of different locations of vesicles within the grid.

C.3.4. Distributions of vesicle locations

As a simple distribution of vesicles we assumed that vesicles are located at random anywhere on the membrane, i.e. anywhere within the grid of channels. The predicted release probability of the terminal is then given by the average release probability across all locations in the grid (termed $RP_{terminal}$). Assuming such a distribution, $RP_{terminal}$ in the control condition is nearly constant for all d. However, the predicted efficiency of exogenous buffers in suppressing phasic release changes by more than two orders of magnitude (Figure C-2 C and D). When compared to experimental data, results for EGTA (both parameter sets) as well as for BAPTA show: d is likely to be at least 250 nm. Otherwise, the expected effect of either exogenous buffer would be far stronger than observed experimentally. To eliminate the uncertainty introduced by the role of ATP (whose kinetic parameters and concentration in the native terminal are uncertain), we repeated the simulations without ATP and simulated the effect of BAPTA and endogenous fixed buffer alone (50 µM vs. 1 mM BAPTA; see below for role of endogenous fixed buffer). Results also imply d > 250 nm.

For large diffusion distances d, $I_{Ca,\,peak}$ per channel in the simulation is > 1 pA. 1 pA is about 5-10 times higher than the usual upper estimates for single calcium channels at the calyx of Held (e.g. Borst and Sakmann, 1996). For large d, therefore, we replaced each single channel with a cluster of 10 closely grouped channels, each conducting only 1/10 of the original channel (channel to channel distance within cluster ~ 15 nm). Predicted effects of exogenous

buffers remained almost unchanged (not shown). The [Ca^{2+}] signal provided by a single, large channel is, for many quantitative arguments, indistinguishable from that of a tight cluster of channels. Henceforth, we will refer to either as a calcium source.

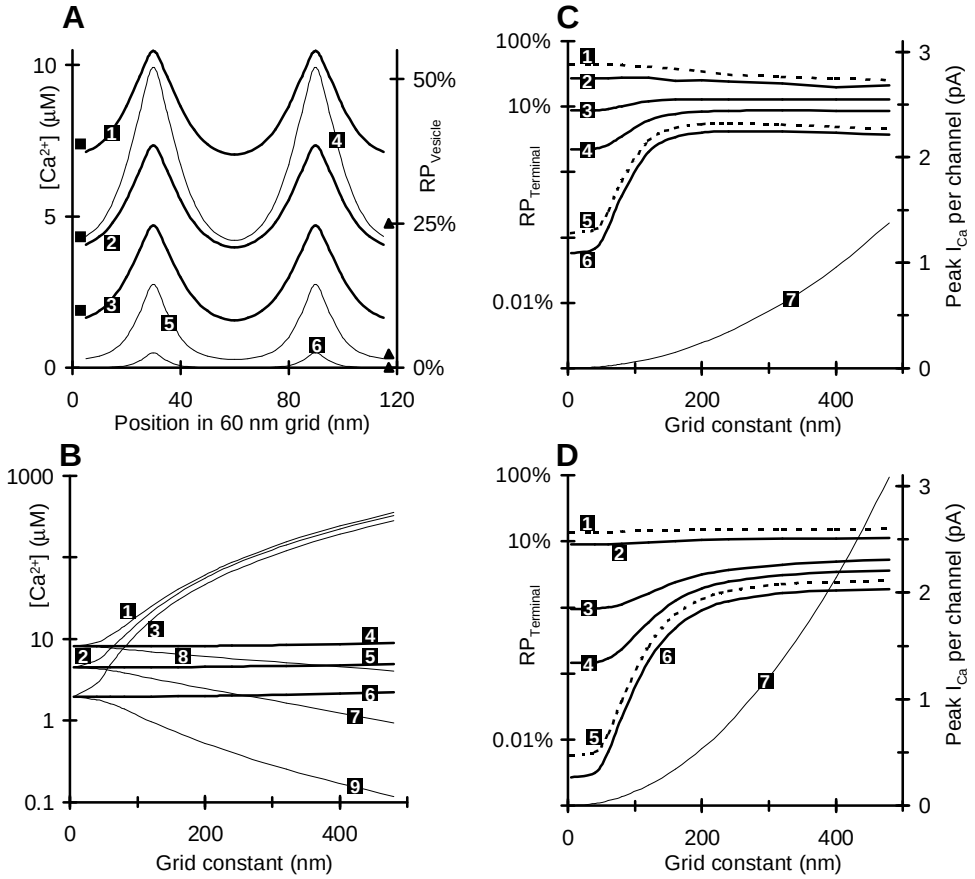

Figure C-2. Effect of channel spacing on release probability.

(A) Spatial profiles of [Ca^{2+}] (traces 1 - 3; snap shot at time of peak I_{Ca}) and of release probability per vesicle ($RP_{vesicle}$) (traces 4 - 6, after 5 msec, right axis) in a d = 60 nm regular grid of channels, under different buffer conditions; channels are at 30 nm and 90 nm (Release Model A). 1, 4: endogenous fixed buffer (EFB), ATP (control condition). 2, 5: EFB, ATP, and 10 mM EGTA. 3, 6: EFB, ATP, and 1 mM BAPTA. Squares at left axis indicate average [Ca^{2+}] across membrane (7.4 µM, 4.3 µM, 1.9 µM for control, EGTA, BAPTA respectively); triangles at right axis indicate average $RP_{vesicle}$ across membrane (25%, 2.4%, 0.13% for control, EGTA, BAPTA respectively). (B) Peaks of [Ca^{2+}] transients for different grid constants and buffer conditions (1, 4, and 7; 2, 5, and 8; 3, 6, and 9 as in A; single channel conductance as in C; Release Model A); traces 1 - 3: peak of transient at 10 nm above a channel. Traces 4 - 6: peak of average transient across all locations in the grid. Traces 7 - 9: peak of transient at half grid constant from two neighboring channels. (C) Predicted average $RP_{vesicle}$ across grid, as a function of the grid constant (Release Model A). Traces 1 - 6 show $RP_{terminal}$ for 6 different buffer conditions. 1: EFB, 50 µM BAPTA, 2: EFB, ATP (= control condition). 3: EFB, ATP, 10 mM *slow* EGTA. 4: EFB, ATP, 10 mM EGTA. 5: EFB, 1 mM BAPTA. 6: EFB, ATP, 1 mM BAPTA. 7: peak I_{Ca} per channel required to achieve $RP_{Terminal}$ ~ 25% for the control condition (right axis). (D) Same as C when using Release Model B. $RP_{terminal}$ ~ 10% for control condition. Results show that channels (or channel clusters) appear to be separated by diffusion distances of > 250 nm (Conclusion II).

C.3.5. Summary and discussion of Conclusion II

In summary, we find as conclusion II: For any hypothesized location of vesicles within a large field of channels or channel-clusters, the average distance between neighboring calcium sources is likely to be > 250 nm. Assuming a current of about 0.1 pA for each calcium channel (Golasch et al., 1992), the whole cell calcium current (2.4 nA) corresponds to 24,000 calcium channels. Distributing these evenly on the membrane (2000 μm^2) would result in a typical distance of about 300 nm between neighboring channels. If there are more channels (with smaller conductance), conclusion II suggests that they are grouped into calcium sources such that large diffusion distances > 250 nm between sources are maintained.

Our result, at a first glance, may seem to contradict previous interpretations of exogenous buffer experiments for the calyx of Held. Previously, a substantial effect of the kinetically slow buffer EGTA in suppressing RP – particularly when compared to effects of faster BAPTA – was used to infer large diffusion distances for calcium between release controlling channels and vesicles (Borst and Sakmann, 1996). This is true in the case of a single domain scenario: The larger the distance from a single calcium source, the stronger the predicted relative reduction of phasic release by mobile buffers (Neher, 1998a; as seen in Figure C-1 B). However, for the case of a large grid of channels, the effect is more complicated. The larger the grid distance *d*, i.e. *the larger the average diffusion distance* between a vesicle and its nearest channel, *the less efficient* buffers are in reducing phasic release. This can be understood by approximating $[Ca^{2+}]_{peak}$ by adding up, for any one location in the grid, the single domains of all other channels (linearized, steady state approximation, Neher, 1998a). The smaller d, the more spatially uniform are the $[Ca^{2+}]$ transients (along the membrane), and thus the more dominated not only by a single, nearby channel but by a large number of channels, located at distances larger than d itself. In addition, since RP is a non-linear function of $[Ca^{2+}]$, it is not sufficient to consider the effect of exogenous buffers on $[Ca^{2+}]$ alone. Instead, when considering distributions of vesicle distances, the buffers' effect on the average release probability must be considered as well. (As seen in Figure C-2 B, the buffers' effect on the average $[Ca^{2+}]$ is independent of d whereas the effect on average RP changes by more than two orders of magnitude.)

Conclusion II regards primarily the probable location of calcium sources with respect to other calcium sources, not to the location of vesicles. As shown, inferring diffusion distances

between channels and vesicles from exogenous buffer experiments depends on *prior* assumptions on how many calcium channels contribute to the local $[Ca^{2+}]$ at the vesicle (single channel domain vs. multiple channels). Therefore, we will address the question of how many calcium channels control the release of individual vesicles in a separate, independent argument (Conclusion III).

C.4. CONCLUSION III: THE MAJORITY OF VESICLES IS CONTROLLED BY CLOSELY GROUPED CLUSTERS OF CIRCA 10 OR MORE CHANNELS

Experimental modification of the stochastic gating of Ca^{2+} channels and/or their partial blockage by toxins affect phasic transmitter release at the calyx of Held (Table C-2). Such experiments have been used to conclude that the majority of vesicles at this synapse is controlled by more than one channel (Borst and Sakmann, 1999a; Wu et al., 1999). Extending these results, we estimated how many calcium channels are likely to control the release of a single vesicle and how these channels appear to be located.

C.4.1. Simplified model

We start with a simple model which assumes (Quastel et al., 1992): (1) Every vesicle's release probability ($RP_{vesicle}$) is equal to the k-th power of $[Ca^{2+}]$ sensed by the vesicle ($[Ca^{2+}]_{vesicle}$). We assume k = 3 (average apparent supra-linearity from experiments, Table C-2). $[Ca^{2+}]_{vesicle}$ is supplied by one or more channels controlling the release of the vesicle. (2) The total number N of channels controlling each vesicle, open or close, is the same at every release site. (3) During an action potential, a channel either opens (probability p) or remains closed (no multiple opening). (4) Each open channel contributes the same $[Ca^{2+}]_{channel}$ to $[Ca^{2+}]_{vesicle}$. Assuming that sites are independent, we get: $RP_{terminal} = (RP_{vesicle})_{average} \propto \Sigma_{i=1}^{N} p(i) \cdot i^{k}$, where p(i) is the probability that, at any single site, i of the N channels open during an action potential.

C.4.1.1. Measuring m: Reducing calcium influx by reducing the channel open probability

As channel gating is stochastic, the number of open channels at each release site varies around p·N, thus causing a variance in $[Ca^{2+}]_{vesicle}$ across sites. Therefore, only the average $[Ca^{2+}]_{vesicle}$ of all release sites is reduced proportionally to p. Since k > 1, the effect on release is non-linear, i.e. the average release probability of all vesicles in the terminal ($RP_{terminal}$) is not proportional to the average $[Ca^{2+}]_{vesicle}$ raised to the k-th power . Instead, $RP_{terminal} \propto p^{m}$. (The notation of m follows the one in Wu et al., 1999; defined in Table C-2.) Therefore, the

apparent degree of supra-linearity of release vs. Ca^{2+} influx measured in actual experiments may be different from k. The discrepancy of m vs. k is the higher, the higher the relative variance in $[Ca^{2+}]_{vesicle}$ across release sites. This relative variance (noise), which depends on the number of Ca^{2+} channels per site, is largest for the case of a single channel: For N =1 , m = 1, independent of k (Augustine et al., 1991). As the number of channels controlling each site increases, the noise in $[Ca^{2+}]_{vesicle}$ across release sites decreases and m approaches k.

C.4.2. Comparison to experiments

In recordings from the calyx of Held, Borst and Sakmann (1999a) reduced the opening probability p for Ca^{2+} channels by means of modified action potential waveforms. To simulate their experiments with the above simple model, we reduced p from 69% (control condition) to 42% (both p given by Hodgkin-Huxley model fitted for calyx of Held; Borst and Sakmann, 1998; Figure C-3 A). The results are shown in Figure C-3 C. Based on the experimental finding that m ~ k, we conclude that phasic transmitter release at the calyx of Held, for the majority of vesicles, is likely to be controlled by at least 10 channels per vesicle. (The experiments by Wu et al. (1999) who used toxins to reduce the number of functioning Ca^{2+} channels, can be interpreted by the same model.) Although, in the above model, the value m is a function of p (high vs. low), the inferred minimum number of channels N is insensitive to the exact values for p. We also tested p = 75% vs. 25% (yielding N_{min} ~ 11) and p = 20% vs. 10% (yielding N_{min} ~ 14).

C.4.3. Full diffusion model

The simplified model above neglects time-dependent buffered diffusion of Ca^{2+} as well as the exact, time-dependent response of vesicles to variable, transient $[Ca^{2+}]$. To confirm our conclusion, we implemented stochastic channel gating into the 3-dimensional, time-dependent model used in I and II. Vesicles and clusters of calcium channels at different sites were located as described for the calculations shown in chapter D. Using pseudo-stochastic sampling, time course and amplitude of the Ca^{2+} current were varied across channels (2-gate Hodgkin-Huxley model, see section B.3). To measure m predicted by the model, channel kinetics were driven either by the physiological action potential waveform (control, p = 69%) or by a modified, step-like waveform (p = 42%, Figure C-3 A). Total conductance per channel cluster was 5.1 pS, or 5.1 pS/N per channel. (5.1 pS is 0.35 of the conductance used to

simulate release at control conditions. The lower conductance, which simulates lower [Ca^{2+}] in the extra cellular solution, was used so that n_{model}~ 3; Figure C-3 D.)

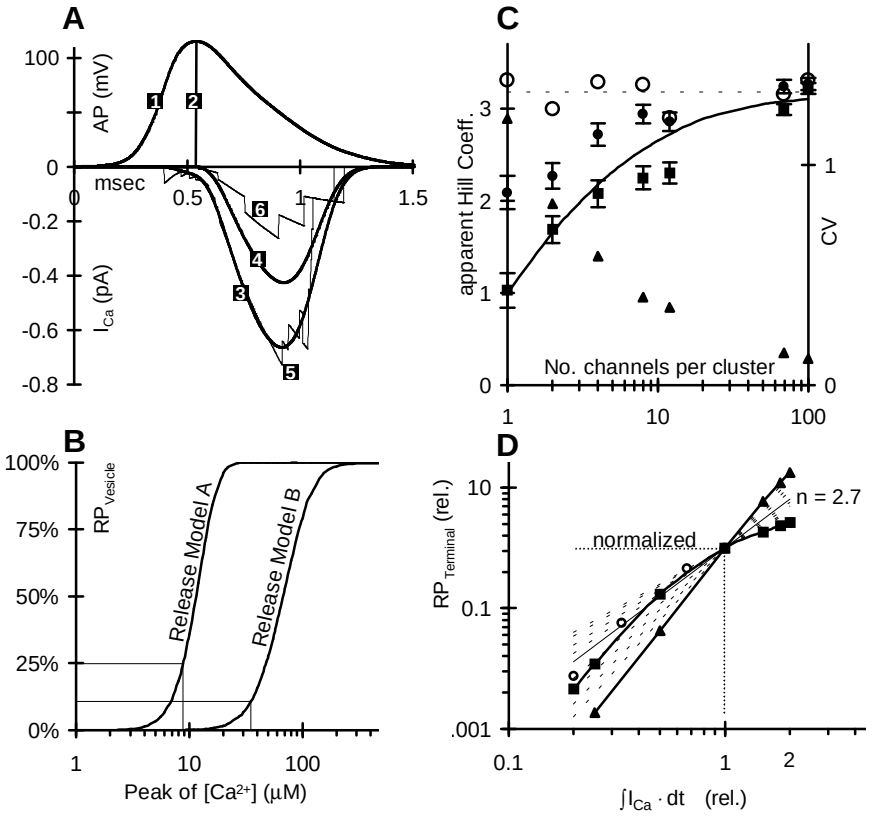

Figure C-3. Effect of number of channels on release probability.

(A) Hodgkin-Huxley Model used to predict I_{Ca} for different action potential (AP) waveforms. 1: physiological AP (+80 mV - 36 mV; shifted on plot). 2: step AP to reduce channel open probability. 3: average I_{Ca} (Release Model A) for 12-channel cluster (phys. AP), half-width of I_{Ca} = 383 µsec, channel open probability p = 69%. 4: same as 3 but for step AP, p = 42%. 5: single stochastic I_{Ca} for 12 channel cluster (phys. AP). 6: same as 5 but for step AP. (B) RP for single vesicle when exposed to a [Ca^{2+}] transient whose time course is equal to that of whole cell I_{Ca} (fwhm 383 µsec). Thin lines indicate release probability during action potentials, according to Release Model A (Bollmann et al., 2000) or B (Schneggenburger and Neher, 2000). (C) Effects of number of channels per cluster on apparent Hill Coefficients m and n. solid line: m with simplified model; solid squares: m with stochastic I_{Ca}; error bars indicate SEM after 400 Monte Carlo simulations for each data point; solid circles: n with stochastic I_{Ca}; error bars indicate SEM after 50-200 Monte Carlo simulations for each data point; triangles: coefficient of variation for the total Ca^{2+} influx (p = 69%, right axis); open circles: m when using average I_{Ca}. (D) Predicted n for two topographies are compared with experimental data (Table C-2). squares: 12-channel-cluster; open circles indicate n when modeled with stochastic channel $I_{Ca}(t)$ (not plotted where indistinguishable from squares; SEM after 200 Monte Carlo simulations smaller than dimension of circles); triangles: grid (d = 60 nm); solid thin line indicates slope 2.7, broken lines indicate range of slopes in experimental studies (2.2 - 4). Results (C) show that release controlling channels are probably organized in tight clusters of ~ 10 or more channels each (Conclusion III).

When channels were gated by the step-like action potential, the total influx into the terminal was 61% of that under the physiological action potential (independent of N). However, the average release probability $RP_{terminal}$ was not reduced to 0.61^3, but instead to 0.61^m. m was strongly dependent on N. We show results for 7 scenarios with N varying between 1 and 100

channels per cluster (Figure C-3 C). The location of channels relative to each other was as follows (positions as x-y co-ordinates in nanometers relative to midpoint of the cluster). N_1: (0,0); N_2: (0,10) and (0,-10); N_4: N_2 plus (10,0) and (-10,0); N_8: N_4 plus (-15,-15), (-15,15), (15,-15), (15,15); N_{12}: N_8 plus (0,20), (0,-20), (20,0), (-20,0). N_{69}: 69 channels distributed evenly on a circle with ca. 50 nm diameter (1 channel per 5 x 5 nm^2). N_{100}: all 100 channels located on the same 5 x 5 nm^2 patch (unrealistic channel density).

To confirm that the predicted change in m was due to the change in noise (Figure C-3 C, right axis) of the total Ca^{2+} influx per cluster – and not due to different channel-vesicle distances inherent in clusters of varying N – we repeated the simulations for all 7 clusters. This time we did not vary individual channel currents stochastically but used the same, average I_{Ca} for every channel (average I_{Ca} as given by the Hodgkin-Huxley Model). As expected, measured m was around 3 for all N (Figure C-3 C). Predictions for m confirm the general finding concluded from the above, simplified model. However, for N = 4 - 12, an additional effect is revealed. Since the channels in the cluster cannot all be in the same place, the diffusion distance to the vesicle they control varies and thus the $[Ca^{2+}]$ that each open channel contributes to the combined $[Ca^{2+}]_{vesicle}$ varies as well. Therefore, variable diffusion distances of the channels controlling a particular vesicle raises the noise of $[Ca^{2+}]_{vesicle}$ (for the same N), thus increasing the discrepancy between the measurement of m vs. n (Artalejo et al., 1994).

C.4.3.1. Measuring n: Reducing calcium influx by reducing the single channel conductance

A second, in fact more traditional way to reduce the average $[Ca^{2+}]$ reaching a vesicle is to simply reduce the concentration of calcium ions in the extra cellular solution. At the calyx of Held, this results in a measured supra-linearity of $RP_{terminal}$ vs. total calcium influx of n ~ 2.7 (n varies for different studies, see Table C-2). Like m, n does not depend on the intrinsic supra-linearity of release vs. $[Ca^{2+}]_{vesicle}$ alone (k in the above notation), but also on the noise in $[Ca^{2+}]_{vesicle}$. We simulated predicted n as a function of N by the stochastic/full diffusion model. Channel clusters for different N were the same as described in section C.4.3. Reduced $[Ca^{2+}]$ of the extra cellular solution was simulated by reducing the single channel conductance in the Hodgkin-Huxley-Model, from 5.1 pS per cluster (control) to 0.61·5.1 pS per cluster. As expected, predicted n depended on N (Figure C-3 C). Results confirm our finding that N is likely to be at least 10.

C.4.4. Summary and discussion of Conclusion III

In summary, we conclude that N ~ 10 or more Ca^{2+} channels control phasic release at the majority of release sites at the calyx of Held, and further that these channels are located at similar distances from the vesicle they control. (For the N = 12 cluster scenario in Figure C-3 C, the average vesicle – located at 118 nm from the cluster center - is located at 90 nm (near side of cluster) to 140 nm (far side of cluster) from an individual channel.) It should be noted that the above calculations are based on the assumption that the Hodgkin-Huxley Model is a sufficiently accurate description for single calcium channel currents. The model is probably not accurate for all Ca^{2+} channel sub-types. Just as variable distance between channels and vesicle increases the noise in $[Ca^{2+}]_{vesicle}$ (see above), different sub-types of Ca^{2+} channels with presumably different conductances produce the same effect: the discrepancy between m and k increases (for the same N). Hence, our estimate N ~ 10 may be viewed as a lower limit.

C.5. CONCLUSION IV: PHASIC RELEASE IS CONTROLLED BY ONE OR A FEW CHANNEL-CLUSTERS PER ACTIVE ZONE - VESICLES ARE LOCATED AT VARIABLE DISTANCE FROM THE CLUSTER

Conclusions I-III represent three independent constraints on the functional topography of channels and vesicles at release sites. On their own, they cannot determine the topography. Each constraint would be satisfied by several different hypothetical topographies. In combination, however, conclusions I-III provide a specific picture of the relative location of calcium channels and vesicles likely to operate at the calyx of Held. This will be shown below.

C.5.1. Combining conclusions I-III

EM-Data of the calyx of Held shows that active zones are separated by 200 - 800 nm from the next, closest zone (Table C-1). The average radius of an active zone is 125 nm. Conclusion II, therefore, suggests that phasic release, for the majority of active zones, is controlled by a single source of calcium per active zone (a source being a single channel or a closely grouped cluster of channels; Figure D-1). Conclusions I and III suggest seemingly contradicting properties of the topography. Experiments using exogenous buffers suggest heterogeneity (distance varies), whereas experiments using reduced open probability of channels suggest

homogeneity (distance is similar). However, the heterogeneity concerns the distance that different vesicles have to the Ca^{2+} source that controls their phasic release. The homogeneity concerns the distances that any one vesicle has to the several channels controlling its release. Conclusion III shows that, at each active zone, vesicles are controlled by several channels (~ 10 or more) and that these channels are located at similar distances from the vesicle they control. In light of this constraint, our scenario involving a closely grouped cluster of ~ 10 channels is an anatomical compromise: A large number of channels which are nevertheless confined to a small region (diameter ~ 50 nm). Thus, the distances between each channel and an individual vesicle located at some distance away from the cluster are similar. 10 Ca^{2+} channels on a circle with 50 nm diameter correspond to one channel per 14 x 14 nm^2 membrane area. This is consistent with EM-measured channel to channel distances at other synapses (Stanley, 1997).

C.5.2. Alternative, but unlikely topographies

Conclusion III, if viewed on its own, would be consistent with another topography: A vesicle located inside a ring-like cluster of channels (or a ring of vesicles around a cluster of calcium channels), such that each channel is located at similar distance from the vesicle it controls. Conclusion I, however, makes this topography appear unlikely. Vesicles appear to be located at a range of distances to channels controlling their release. Therefore, equidistant co-localization of a majority of vesicles with channels (as inside a ring) seems unlikely. Similarly, it appears unlikely that phasic release, for the majority of active zones, is controlled by more than one or a few channel clusters, each with a possibly smaller number of channels. More than one spatially disjunct calcium sources per active zone would decrease the heterogeneity of distances between vesicles and their calcium source(s) (conclusion I). In addition, more than one cluster would decrease the homogeneity of distances of an individual vesicle to its release controlling channels. To satisfy conclusion III (low noise of $[Ca^{2+}]$), the decrease in homogeneity would have to be counteracted by increasing the total number of channels per active zone. This would decrease the required single channel conductance (1.2 pS, if one cluster with 12 channels) to unreasonably low levels. Finally, to demonstrate that the clustering of calcium channels is required at all, we tested the following alternative topography: 12 calcium channels are spread out evenly over each active zone. Each active zone is a circle with 125 nm radius. The location of channels was as follows (in nm relative to center of circle): 4 channels at (±90,±30); 4 channels at (±30,±90); 4 channels at

(±30,±30). Vesicles were located at random on the active zones. To yield $RP_{terminal}$ = 25% for the control condition, a single channel conductance of 0.98 pS was required. With respect to conclusion III, the apparent Hill Coefficient for this topography was n = 3.4 when using average $I_{Ca}(t)$ (same for each channel); n = 2.6 ± 0.1 when using stochastic $I_{Ca}(t)$ (different for each channel), and m = 1.9 ± 0.1 (mean ± SEM, after 400 Monte Carlo simulations). In comparison to experiments, the result for m seems low, but cannot be viewed as conclusive evidence against the alternative topography. With respect to exogenous buffers, however, addition of 10 mM EGTA reduced predicted RP to 9.3%, and of 1 mM BAPTA to 1.5%. The strong effect of 1 mM BAPTA, whose predicted RP is 6 times stronger than that observed experimentally, makes the hypothesized, alternative topography very unlikely to be present at the majority of active zones at a real calyx of Held.

D. PHYSIOLOGICAL CALCIUM SIGNALING AND FUNCTIONAL SIGNIFICANCE OF RELEASE SITE TOPOGRAPHY

In chapter D, we show simulated time courses of presynaptic [Ca^{2+}] transients and release probabilities for vesicles during transmission at the calyx of Held. The simulations are based on a hypothesized release site topography which is in compliance with the findings in chapter C, and which we propose as the topography most likely to be found at a real calyx of Held terminal. The results demonstrate key features of physiological calcium signaling during fast synaptic transmission at this synapse. In addition, results will demonstrate the significance of the proposed topography for the specific functional characteristics of this synapse – high fidelity transmission at frequencies of up to several hundred Hertz.

D.1. IMPLEMENTATION OF THE INFERRED TOPOGRAPHY IN THE MODEL

Complying with the topographical characteristics of release sites inferred for the calyx of Held (conclusion IV), we implemented the following relative location of vesicles and calcium channels on active zones in the model terminal. This topography was used for all further calculations. All numbers given in the following text apply to the simulations using Release Model A, unless indicated otherwise.

D.1.1. Location of calcium channels

At each active zone, a single cluster of Ca^{2+} channels controls phasic release. The cluster has a diameter of ~ 50 nm. It consists of 12 channels (Figure D-1 B), with a conductance of 1.21 pS per channel. 1.21 pS corresponds to an average $I_{Ca,\,peak} = 0.055$ pA per channel during physiological action potentials. The cluster is located at random anywhere on each active zone. Based on the EM-data (Table C-1), individual active zones in the simulation are circles of variable size, with a radius varying around $r_{average} = 125$ nm, $\sigma = 31$ nm (distribution of radius is gaussian).[39]

D.1.2. Location of vesicles and distance distribution function

(Readily releasable) vesicles are located at random anywhere on every active zone (except for whichever space is already occupied by the channel-cluster). The random location of vesicles

[39] The symmetric radius distribution with $\sigma_{radius} = 31$ nm results in a skewed area distribution of active zones, with σ_{area} as determined by the EM-reconstructed morphology (Lübke et al., 2001). Assuming each active zone to be a perfect circle is a good approximation to the actual, patch-like structure of active zones at the calyx of Held.

was chosen for lack of direct evidence of any other spatial organization. As a consequence of the large active zones, the distance between a vesicle and the cluster (mid-point) ranges between 30 nm and 300 nm (mode = 90 nm, mean = 118 nm, σ = 59 nm, non-symmetric; Figure D-1 A). The exact number of readily releasable vesicles per active zone is irrelevant to our simulation (about 1-3, Table C-1). The distribution function was constructed by a Monte Carlo process,[40] consisting of the following steps: (1) pick a circle with radius from a distribution N (mean 125 nm, σ 31 nm). (2) pick a point A anywhere on that circle. (3) pick a second point B anywhere on the same circle (independent of point A). The distribution of distances is given by all randomly generated distances between spots A and B.[41] In the final distribution function, weights for any distance < 30 nm were set to zero, reflecting the assumption that no vesicle can be located closer than 30 nm to the center of the channel cluster (as this would place the vesicle in-between calcium channels).

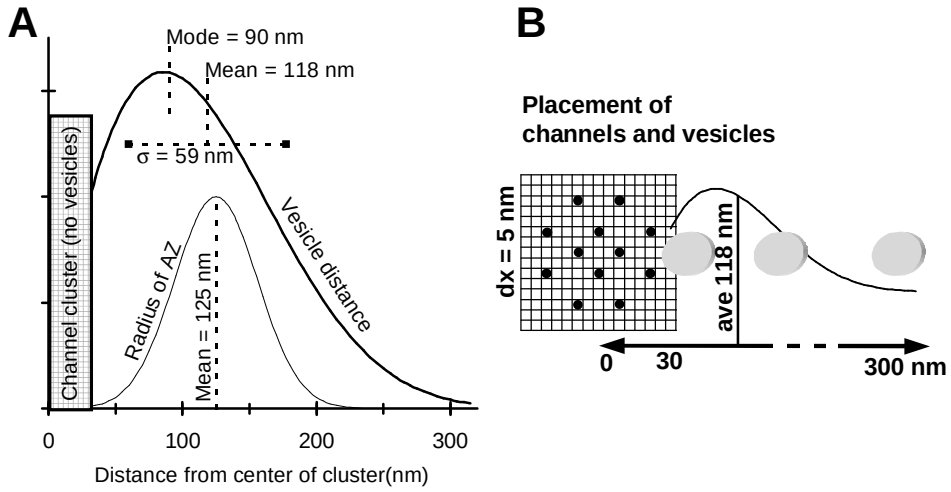

Figure D-1. Relative location of channels and vesicles across different release sites.

(A) The distribution function is the result of random location of channel clusters (one per active zone) and vesicles (1-3 per active zone) anywhere on the active zones (circles of varying size, average radius 125 nm). The channel cluster spans to about 25 nm from its center; assumes that no vesicle is located closer than 30 nm from center See text for further explanation. (B) Location of 12 channels (= calcium entry points in buffered diffusion model) as used for all simulations shown in chapter D (note that panel B is not drawn to scale).

D.1.3. Contribution of other Ca^{2+} channels

In our model, the total current during an action potential from 600 Ca^{2+} channel clusters (one cluster per active zone) is $I_{Ca,\ peak}$ = 0.41 nA. This is 17% of the whole cell current observed in experiments at the calyx of Held ($I_{Ca,\ peak}$ = 2.4 nA, Table C-1). Around the channel-cluster at

[40] Random number generator *ran(2)* as referenced in chapter B.

[41] Randomly generated distances were sorted into a histogram (0-340 nm, dx = 5 nm, as in model). The Monte Carlo process was iterated until each bin content was within 0.1% accuracy of the final, converged result.

each active zone, 0.41 nA gives rise to localized domains of [Ca^{2+}] which trigger the release of $RP_{terminal}$ = 25% of all readily releasable vesicles (same as observed in experiments). (When using the Release Model B, the respective numbers are 1.01 nA, 42%, and $RP_{terminal}$ = 10%). In the simulation, the remainder of the calcium current does not locally enter through explicit Ca^{2+} channels but, instead, adds to the volume average [Ca^{2+}], raising it to the same level as that measured in experiments. The model thus indirectly accounts for contributions to [Ca^{2+}] from additional channels that are not directly accounted for by the channel clusters on the active zones (see section B.2.2.3). Many such Ca^{2+} channels will be located on the unspecialized membrane away from active zones, thus not raising the local [Ca^{2+}] sensed by the vesicles. Even though some additional channels might be located on active zones themselves (in addition to the channel clusters), their role in triggering phasic release is probably marginal. If it were not, such calcium channels, by virtue of conclusions I-IV, would have to be part of the clusters already included in the model. (Note that our model does not include any contribution to [Ca^{2+}] from possible release of calcium from intracellular stores. At the calyx of Held, this contribution, during a single action potential, is marginal at most (Helmchen et al., 1997).)

D.1.4. Implied estimates for the density of calcium channels

Our model implies estimates of the Ca^{2+} channel density of the active zone in comparison to that of the unspecialized presynaptic membrane. Active zones make up 2% of the total presynaptic membrane (40 μm^2 of 2000 μm^2, Table C-1), while Ca^{2+} channels confined to active zones contribute 17% of the total Ca^{2+} influx. This implies that the density of channels on active zones is about 10 times higher than that on the unspecialized membrane (assuming similar conductance for all channels). (When using the Release Model B, the respective factor is 36). Assuming 12 channels per cluster, the channel density per average active zone (0.052 um^2) is 231 per um^2. The implied total number of Ca^{2+} channels in the terminal is ~ 43,000 (17,000 when using Release Model B). Note that these estimates depend on the whole cell I_{Ca}, membrane area, and the size of active zones. All three parameters may vary from terminal to terminal. However, the above conclusions on the likely topography of release sites do not depend on the exact values of these parameters (see discussion in section E.1). A concentration of calcium channels at active zones is in agreement with experimental studies which have measured regions of locally elevated [Ca^{2+}] at presynaptic release sites, but whose spatio-temporal resolution was too low to identify calcium domains

of individual channels (Llinas et al., 1992; Tucker and Fettiplace, 1995; DiGregorio et al., 1999; Sugimori et al., 1994; Roberts et al., 1990).

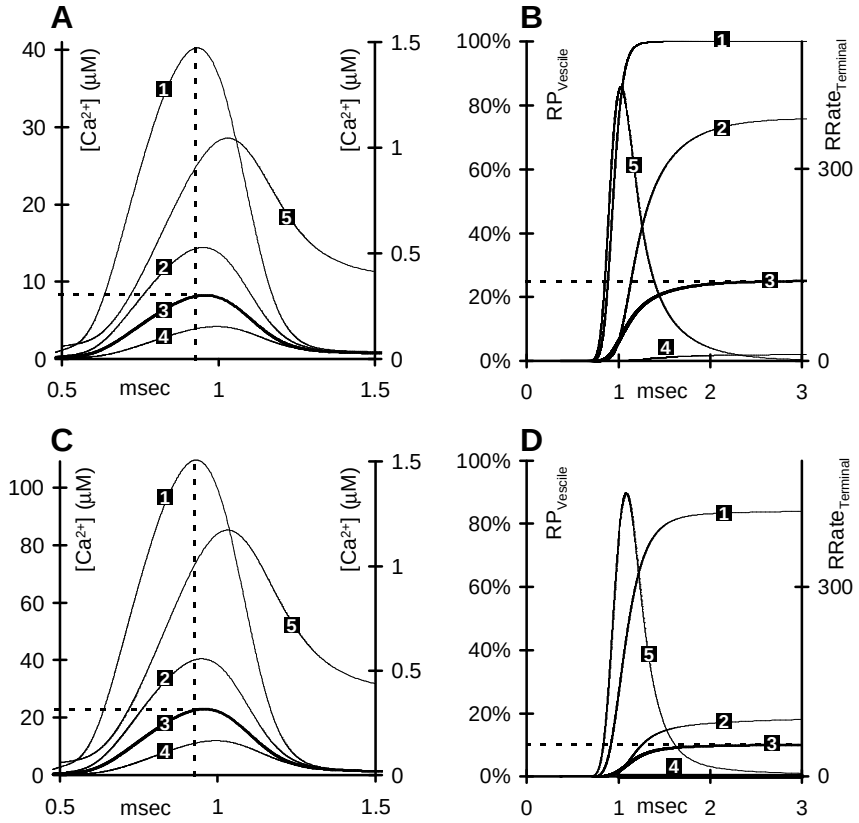

Figure D-2. Physiological [Ca^{2+}] signaling. Heterogeneity of distances, [Ca^{2+}] transients, and RP.
(A) Time course of [Ca^{2+}] for vesicles at different distances from channel cluster (Release Model A). 1: 30 nm from center of cluster; 2: 60 nm; 3: average over all vesicles, peak = 8.2 µM, half-width = 391 (fwhm) µsec; 4: 120 nm; 5: volume average [Ca^{2+}] (right axis); vertical dashed line indicates time of peak I_{Ca}. (B) Time course of cumulative release probability for single vesicle (RP) at different distances; 1, 2, 4: same distances as in A; 3: average of RP across all vesicles ($RP_{5\,msec}$ = 25%). 5: release rate of terminal (assuming pool size 800; right axis). (C) Same as A but using Release Model B. 3: peak = 23.0 µM, half-width = 384 µsec. (D) 1, 2, 4: Same as B but using Release Model B (4 merged with x-axis); 3: $RP_{5\,msec}$ = 10%. 5: assuming pool size 2000; right axis.

D.2. HETEROGENEOUS RELEASE PROBABILITY AND PHYSIOLOGICAL CALCIUM SIGNALING

In our model, vesicles at different distances from calcium channels sense [Ca^{2+}] transients of different amplitude and time course. In our simulation for single, physiological action potentials, $[Ca^{2+}]_{peak}$ varies between 40 µM for vesicles closest to the channels (30 nm from cluster center), and 0.5 µM for the very few vesicles furthest away. The peak of the average transient (across all vesicle locations) is 8.2 µM. It has a half width (fwhm) of 391 µsec (Figure D-2 A). As a result of the variation in [Ca^{2+}], the probability of a single vesicle to contribute to

phasic release in response to an action potential varies as well, in our simulations between $RP_{vesicle}$ = 100% and $RP_{vesicle}$ = 0.006% (Figure D-2 B).

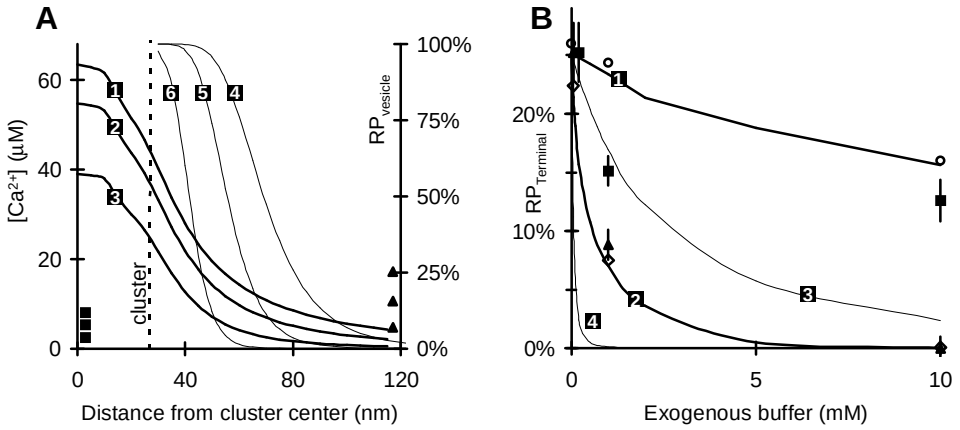

Figure D-3. Heterogeneous release probability and effects of exogenous buffers.
(A) Spatial profiles of $[Ca^{2+}]$ (traces 1 - 3; snap shot at time of peak I_{Ca}) and of release probability per vesicle ($RP_{vesicle}$) (traces 4 - 6, after 5 msec, right axis) under different buffer conditions (Release Model A); single cluster with 12 channels centered at distance 0 nm, extending to distance 25 nm (vertical dashed line). 1, 4: endogenous fixed buffer (EFB), and ATP (control condition). 2, 5: EFB, ATP, and 10 mM EGTA. 3, 6: EFB, ATP, and 1 mM BAPTA. Squares at left axis indicate average $[Ca^{2+}]$ across all vesicles (8.1 µM, 5.4 µM, 2.5 µM for control, EGTA, BAPTA respectively); triangles at right axis indicate average $RP_{vesicle}$ across all vesicles ($RP_{terminal}$), 25%, 16%, 7.1% for control, EGTA, BAPTA respectively. (B) Predicted buffer dose responses for $RP_{terminal}$ (Release Model A). Two topographies (channel cluster vs. channel grid, d = 60 nm) are compared with experimental data (squares: EGTA, triangles: BAPTA; mean ± SEM; Table 2). 1: EGTA (cluster); open circles show results using stochastic I_{Ca}, SEM after 100-200 simulations smaller than dimension of circles. 2: BAPTA (cluster); open diamonds show results using stochastic I_{Ca}, SEM after 100-200 simulations smaller than dimension of diamonds 3: EGTA (grid). 4: BAPTA (grid). Results illustrate how heterogeneous location of vesicles explains measured effects of exogenous buffers (see text) but not if vesicles are located within in a dense grid of channels (conclusion I and II).

Essentially, considering variable distance of vesicles constitutes a departure from the concept of a single, or average physiological $[Ca^{2+}]$ transient driving phasic transmitter release. Likewise, by definition of the non-linear response of release vs. $[Ca^{2+}]$, the search for an average distance of vesicles to channels is rendered somewhat futile. In our simulations, the average distance of a vesicle to the center of the channel cluster is 118 nm (across all vesicles and active zones in the terminal). However, a vesicle actually located at 118 nm from a cluster does not have the average release probability of all vesicles in the terminal $RP_{terminal}$ = 25%, but only $RP_{vesicle}$ = 2% (Figure D-3 A, right axis). Neither can one define an effective or typical distance. To achieve $RP_{vesicle}$ = $RP_{terminal}$ = 25%, a vesicle must be located at 80 nm from the channel cluster. Here, our model predicts a roughly bell-shaped transient peaking at $[Ca^{2+}]_{peak}$ = 8.7 µM (Figure D-3 A, left axis; as estimated by Bollmann et al., 2000). However, this distance leads to confusing results when interpreting effects of exogenous

buffers. In the presence of 1 mM BAPTA, the vesicle at 80 nm does not show the predicted drop in the average release probability to $RP_{terminal}$ = 7%, but to $RP_{vesicle}$ = 0.02%.

D.2.1. Heterogeneity and effects of exogenous buffers

As shown in Figure D-3 B, our model reproduces well the experimentally measured dose response for both BAPTA and EGTA (with the exception of 1 mM EGTA).[42] We will now show why heterogeneous location of vesicles predicts release probabilities as seen in experiments, whereas other, more uniform spatial organizations do not. Variable diffusion distance between release controlling channel-clusters and vesicles creates a pool of vesicles, which consists of a wide mixture of release probabilities. By the same token, calcium buffers affect each of the release probabilities differently, again depending on the diffusion distance for calcium from channels to the particular vesicle. Therefore, the overall net effect on average release $RP_{terminal}$, which is measured in experiments, depends on the distribution of distances between vesicles and channel clusters.

To illustrate the effect, consider the vesicles as three separate groups, according to distance. Close (30 - 40 nm from cluster center), Medium (40 - 70 nm), and Far (> 70 nm). As shown in Figure D-3 A, the release probability of close vesicles is $RP_{vesicle}$ = 100% in response to a single action potential (control, i.e. no exogenous buffers). At 30 - 40 nm, exogenous buffers (1 mM BAPTA as well as 10 mM EGTA) reduce the peak of the calcium transient ($[Ca^{2+}]_{peak}$) to roughly 0.5 of that under control conditions. However, the release probability of the close vesicles remains unaffected, because release is already saturated. This is different for vesicles at medium distance. Again comparing buffer vs. control condition, BAPTA reduces $[Ca^{2+}]_{peak}$ to 0.5, enough to strongly reduce the release probability. However, EGTA, at this distance, reduces $[Ca^{2+}]_{peak}$ less, and the release probability stays high. For far vesicles, finally, both buffers strongly reduce $[Ca^{2+}]_{peak}$. The release probability is reduced even more strongly because the release controlling molecular sensor, at this distance not saturated, responds steeply to changes in $[Ca^{2+}]$. Since the close vesicles are unaffected by reductions in $[Ca^{2+}]$

[42] Although the predicted suppression of RP by 10 mM EGTA is in good agreement with experiments, the dose-dependence is not correctly reproduced. The predicted suppression of RP by 1 mM EGTA *could* be increased (i.e. closer to experiments) by manipulating the assumed distribution function for the distance between vesicles and channel clusters. Different distributions, assuming more complicated organizing patterns of vesicles' locations, would result in a shear infinite number of possible dose response curves. We did not investigate this as this would have meant to deviate from the general approach outlined in section A.2.

whereas other vesicles are affected, the predicted $RP_{terminal}$ in the presence of buffers is in agreement with that observed in experiments. $[Ca^{2+}]_{peak}$, averaged across all vesicles, is 8.2 µM for the control condition, 5.4 µM with 10 mM EGTA, and 2.5 µM with 1 mM BAPTA. The above cluster topography is in contrast to the more homogenous grid scenario we showed in Figure C-2 A. While the reduction of the average $[Ca^{2+}]_{peak}$ by exogenous buffers is similar to that in the cluster scenario, the predicted reduction of $RP_{terminal}$ in the grid scenario is much too strong (see Figure C-2 A for details). In essence, the heterogeneity of vesicle distances inherent in the cluster topography creates a safe harbor for some of the vesicles, such that they are released even if the calcium transients are reduced by exogenous buffers.

D.2.2. Heterogeneity and apparent Hill Coefficient

As described in detail in conclusion II, the location of vesicles and channels affect the measured steep-ness (m, n) at which release probability responds to changes in calcium influx. Figure C-3 C shows how predicted $RP_{terminal}$ changes when influx is varied by reducing the channel open probability ($m = 2.3 \pm 0.1$ for the cluster with $N = 12$ channels as used in all above simulations; mean ± SEM after 400 Monte Carlo simulations). Figure C-3 D shows the predicted reduction in $RP_{terminal}$ when influx is reduced by reducing the single channel conductance (1.21 pS to 0.12 pS, reflecting a reduction in $[Ca^{2+}]$ from 2 mM to about 0.2 mM in the extra cellular solution). The predicted $RP_{terminal}$ depends supra-linearly on the total calcium influx. The predicted slope in the double logarithmic plot (n) increases with decreasing $RP_{terminal}$. The average slope predicted by our model is $n = 2.8$ (in agreement with experiments; Table C-2). Note that the prediction for m, as well as that for n at large conductance, is somewhat lower than that observed in experiments. The reason is that $RP_{vesicle}$ of some vesicles is almost saturated and, therefore, less sensitive to changes in $[Ca^{2+}]$. (Since the kinetic release models we used in the simulations have 5 calcium binding sites with identical forward binding rates, the maximum possible slope is 5.) For comparison, the predicted n for the grid scenario ($d = 60$ nm) is 4.4 (i.e. outside the range observed in experiments).

D.2.3. Heterogeneity, buffer saturation, and overlap of calcium domains

The question whether phasic transmitter release is controlled by one or by several Ca^{2+} channels per vesicle has been the subject of an ongoing debate. With respect to previous studies of Ca^{2+} channel domains and possible domain overlap, our conclusions for the calyx

of Held are best summarized as follows: Regarding the quantitative effects of exogenous buffers, vesicles essentially behave as if controlled by a single channel domain. Even though the current required in our model ($I_{Ca,\,peak}$ = 0.66 pA) is likely too large to be supplied by a single channel, the combined domain of ~ 10 closely clustered channels is similar to that of a single, large channel. Regarding experiments that reduce the open probability of Ca^{2+} channels, our simulations reproduce the effects inherent in domain-overlap scenarios (discussed in Borst and Sakmann, 1999a). Our calculations reproduce experimental data on differential effects of BAPTA/EGTA in suppressing release without invoking local depletion of unbound BAPTA ('buffer saturation', see Naraghi and Neher, 1997). In our scenarios, mobile buffers deplete only marginally. At the time of peak I_{Ca} and at the center of the channel cluster (where depletion is the strongest), the concentration of unbound BAPTA ($[BAPTA]_{local}$) is 90% of the volume average concentration of unbound BAPTA ($[BAPTA]_{vol}$). Unbound $[ATP]_{local}$ is 94% of unbound $[ATP]_{vol}$. In contrast, unbound endogenous fixed buffer (EFB) is depleted locally. Again at the peak of I_{Ca}, unbound $[EFB]_{local}$ is only 6% of unbound $[EFB]_{vol}$ (all numbers for the 1 mM BAPTA scenario shown in Figure D-3 A).

D.3. SENSITIVITY ANALYSES AND THE ROLE OF ENDOGENOUS BUFFERS

The exact concentrations and binding kinetics of endogenous buffers are not known for the calyx of Held terminal. Our model includes ATP (mobile) as well as one fixed buffer. The fixed buffer simulates the effect of one or more not further identified fixed or very poorly mobile buffers. Potentially, the uncertainty in the kinetic parameters and concentration of these buffers could cause considerable uncertainty of our results. To investigate this, we have changed concentration and binding kinetics of the endogenous buffers to estimate the sensitivity of predicted phasic transmitter release to these parameters. The analysis also serves to clarify the role of endogenous buffers in our model, i.e. their presumed function during physiological calcium signaling at the calyx of Held. The reference scenario for each parameter variation is the cluster scenario shown in chapter D (control condition, $RP_{terminal}$ = 25%). Fixed buffer (EFB): Leaving out the fixed buffer completely (concentration 0 μM) results in $RP_{terminal}$ = 60% within the first 5 msec, and 90% within the first 20 msec. This is expected: Since the only remaining, mobile buffer (ATP) has little buffer capacity (see Helmchen et al., 1997), the 12 μM calcium ions which enter the terminal during an action potential are not buffered, and hence give rise to $[Ca^{2+}]$ ~ 12 μM in the entire terminal. This saturates release for all vesicles. The binding ratio of EFB at the calyx of Held terminal has

been measured to be about 40 (Table C-1). Therefore, any reasonable parameter variation should change only the kinetic properties of the EFB, not the binding ratio. Keeping the binding ratio constant (by adjusting the dissociation constant), we varied the concentration of EFB between 10% and 1000% of the reference value (thereby also changing its buffer product between 10% and 1000%). This changed predicted $RP_{terminal}$ between 40% and 20%, respectively. The analysis shows that EFB – as expected from the fact that it is locally depleted – plays only a minor role in the direct attenuation of the local $[Ca^{2+}]$ transients that control phasic release of transmitter (in comparison, see Roberts, 1994). However, the role of EFB during synaptic transmission at the calyx of Held is nevertheless crucial. It keeps the global volume average of $[Ca^{2+}]$ low, which in turn allows for a rapid decay of local $[Ca^{2+}]$ at release sites once calcium channels close. This serves to turn off phasic release after an action potential, such that only a fraction of the pool of the readily releasable vesicles is released. Endogenous ATP: Since the binding ratio of ATP in native terminals in not exactly known, we investigated two sets of parameter variations for ATP. (1) Keeping the binding ratio constant in each scenario, we changed both the concentration and the dissociation constant between 10% and 1000% of their respective reference values. This changed $RP_{terminal}$ between 37% and 22%, respectively. (2) Keeping the buffer product constant in each scenario, we changed both the concentration and (inversely) the forward binding rate, again between 10% and 1000% of the reference values. This changed $RP_{terminal}$ between 44% (low concentration/high forward rate) and 12% (high rate/low concentration). Complete removal of ATP from the model resulted in $RP_{terminal} = 48\%$. This shows that the role of ATP during synaptic transmission is both global and local (in the above sense), however both roles are minor. For scenarios involving exogenous buffers EGTA or BAPTA, the presence of ATP affects predicted $RP_{terminal}$ even less since the buffer effect is dominated by the higher concentration of the exogenous buffer (as seen in Figure C-2 C and D). Summarizing, even drastic variations in the parameters of endogenous buffers (2 orders of magnitude) do not change predicted $RP_{terminal}$ to a degree that would compromise our conclusions on release site topography.

D.4. FUNCTIONAL RELEVANCE OF PROPOSED TOPOGRAPHY FOR HIGH FREQUENCY TRANSMISSION

D.4.1. Heterogeneity and role of Ca^{2+}-diffusion in synaptic delay

The time of calcium diffusion from channels to vesicles is believed to constitute only a small part of synaptic delay times (Adler et al., 1991; Borst and Sakmann, 1996; Yamada and Zucker, 1992). Our model confirms this view for the calyx of Held, albeit with some qualifications. (Simulations used Release Model A. Analogous calculations using Release Model B yielded similar results; not shown).

D.4.1.1. Direct contribution of diffusion time to synaptic delay

Once Ca^{2+} channels have opened, calcium needs to diffuse to the vesicle (i.e. to its presumably co-localized release controlling molecular sensor). This process is not instantaneous and thus may contribute to synaptic delay. To quantify the effect, Figure D-4 shows the time course of calcium influx through channels, superimposed with the predicted time course of $[Ca^{2+}]$ transients at various distances. As shown for the case of a non-physiological, pulse-like I_{Ca}, the local transient at the channel cluster (30 nm from center) reaches nearly steady state within ~ 100 µsec after onset of the calcium current. In contrast, the average transient (average across all vesicles) as well as the transient at 200 nm have not yet reached their steady state level. In other words, due to buffered diffusion of calcium, the time course of $[Ca^{2+}]$ transients controlling the vesicles would not be able to follow I_{Ca}, if it were pulse-like.

This is different for the case of the physiological, roughly bell-shaped $I_{Ca,\ physiol.}$, as it is generated by a cluster of closely grouped channels that open and close stochastically (time integrals of $I_{Ca,\ pulse}$ and $I_{Ca,\ physiol.}$ were the same). One finds that the local $[Ca^{2+}]$ transient at the channel cluster follows $I_{Ca,\ physiol.}$ almost perfectly (not included in Figure D-4). Even at 200 nm, the peak of $[Ca^{2+}]$ is reached only ~ 150 µsec later than the peak of $I_{Ca,\ physiol.}$ itself. The average $[Ca^{2+}]$ transient follows the time course of $I_{Ca,\ physiol.}$ well, with a small lag of ~ 50 µsec (see also Schneggenburger and Neher, 2000). Thus we estimate that during action potentials at the calyx of Held, the direct contribution of diffusion time to synaptic delay is only ~ 50 µsec. This is aided by the time course of the physiological calcium current itself. Its rise and decay (roughly bell-shaped, half-width (fwhm) 383 µsec) is slow enough to be easily followed by the buffered diffusion system that governs the $[Ca^{2+}]$ transients.

D.4.1.2. Indirect role of diffusion in synaptic delay

We define synaptic delay as the time between onset of I_{Ca} and the onset of the modeled excitatory post-synaptic current (EPSC). Note that the delay time calculated in our model does not represent synaptic delay as it is measured in experiments. This is because the model does not account for additional delays caused by any steps after the kinetic response of the release controlling molecular sensor.[43] The experimentally measured EPSC in Figure D-4 was shifted in time, to allow comparison of the time course (Bollmann et al., 2000). In the following analysis, we will focus on differences in synaptic delay for different $[Ca^{2+}]$ transients rather than on delay times in absolute terms. As for the predicted time course of the EPSCs, we deliberately focused on the rising phases only. This will be motivated further below.

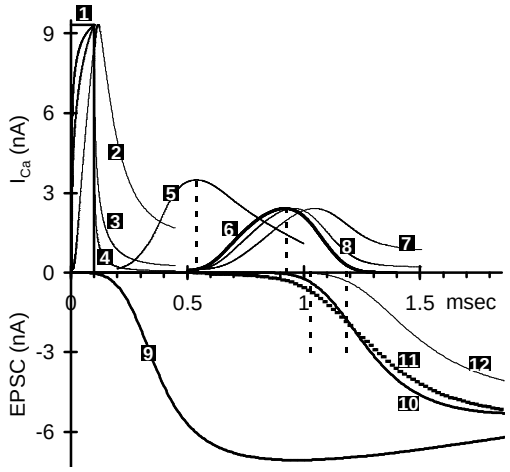

Figure D-4. Functional significance: Synaptic delay.

Role of diffusion in synaptic delay (Release Model A). Predicted EPSCs (bottom) for different I_{Ca} (heavy lines, top). Also shown, time course of $[Ca^{2+}]$ transients at different distances from channel cluster (thin lines, top, relative units, each normalized to the peak of the respective I_{Ca}). See text for further details. 1: Pulse-like I_{Ca}; 2: 200 nm, $[Ca^{2+}]_{peak}$ = 3.6 µM; 3: average across vesicles, $[Ca^{2+}]_{peak}$ = 32 µM; 4: 30 nm, $[Ca^{2+}]_{peak}$ = 167 µM; 5: Action Potential time course (relative units); 6: physiological, whole cell I_{Ca}; 7: 200 nm, $[Ca^{2+}]_{peak}$ = 1.6 µM; 8: average across vesicles, $[Ca^{2+}]_{peak}$ = 8.2 µM; 9: predicted EPSC for pulse-like I_{Ca}; 10: predicted EPSC for physiological I_{Ca}; 11: measured, single EPSC from Bollmann et al., 2000 (time-shifted); 12: EPSC for virtual $[Ca^{2+}]$ transient;. Results show that the average $[Ca^{2+}]$ transient lags physiological I_{Ca} by only ~ 50 µsec, but vesicles located close to channels may shorten synaptic delay (see text).

[43] This would include any steps that are not meant to be 'covered' by the kinetic model: formation of the fusion pore, diffusion of transmitter out of the vesicles and across the synaptic cleft, binding of transmitter to the post-synaptic receptors, and opening of post-synaptic receptors (ion-channels) which results in the recorded, electrophysiological response.

The EPSC for the pulse-like I_{Ca} starts within 100 µsec after onset of I_{Ca} (20%-80% rise time of EPSC is 230 µsec, peak is 7.1 nA; Figure D-4). The short delay is expected from the high $[Ca^{2+}]$ transients and the fast forward binding rates of the release sensor, even though the calcium does not reach all vesicles immediately. For the physiological I_{Ca}, onset of the EPSC (rise time 310 µsec, peak 5.3 nA) is about 400 µsec after onset of I_{Ca} (onset of I_{Ca} is at the peak of the action potential, at 540 µsec). The peak of the average release rate underlying the EPSC (not shown) is at 1030 µsec, or 100 µsec later than the peak of I_{Ca} (third vertical dashed line from left in Figure D-4). For the calyx of Held, this time interval has been measured to be about 5 times larger (~ 500 µsec; Borst and Sakmann, 1996). This confirms that a large part of the physiological delay is caused by steps after the kinetic response of the release controlling molecular sensor.

Bollmann et al. (2000) and Schneggenburger and Neher (2000) have shown that EPSCs at the calyx of Held – when evoked by $[Ca^{2+}]$ uncaged from photo-sensitive chelators – have synaptic delays the shorter, the higher the $[Ca^{2+}]$ signal. In our model, phasic release is comprised of release from vesicles that are located at different distances to channel clusters and which are therefore exposed to $[Ca^{2+}]$ transients of different amplitude (maximum of ~ 40 µM vs. ~ 8 µM for the average). Therefore, we expect that the vesicles in close proximity to channel clusters release neurotransmitter earlier than the average vesicle and thus help to shorten synaptic delay. To quantify the effect, we calculated the EPSC predicted if all vesicles *were* controlled by a single, virtual $[Ca^{2+}]$ transient; i.e. if all vesicles were located at the same distance from calcium channel clusters. As the virtual transient, we chose the average $[Ca^{2+}]$ transient predicted by the diffusion model (average across all vesicles, $I_{Ca,\ physiol.}$; Figure D-4). This calculation essentially removes effects of heterogeneous $[Ca^{2+}]$ transients from the modeled response. The resulting $EPSC_{virtual}$ has a peak amplitude of 4.5 nA (rise time 410 µsec), similar to that predicted by the full diffusion model ($EPSC_{physiol.}$). However, the onset of $EPSC_{virtual}$ is about 150 µsec later than that of $EPSC_{physiol.}$. The peak of the vesicle release rate generating $EPSC_{virtual}$ is at 1182 µsec (Figure D-4, first vertical dashed line from right).

D.4.1.3. Summary and discussion on synaptic delay

In summary, the predictions of our model confirm that the actual time of calcium diffusion constitutes only a small part of synaptic delay (~ 50 µsec). However, a direct contribution of

only ~ 50 µsec does not imply that buffered calcium diffusion does not play a significant role in determining the onset of EPSCs. Instead, the exact time of onset of physiological EPSCs depends on the amplitude of [Ca^{2+}] transients and thus on where vesicles are located with respect to calcium channels. Early onset of the EPSC may be aided by vesicles located close to channels. Recently, it has been shown that synaptic delay times at the calyx of Held shorten during early postnatal development of the synapse (postnatal day 5 - 14; Taschenberger and von Gersdorff, 2000). As the delay times depend – among other factors – on the location of vesicles, the shortening of delay times suggests that the spatial organization of vesicles around release controlling channels may change during early development of this synapse.

D.4.2. Heterogeneity and synaptic fidelity during high frequency transmission

Part of a structure involved in the location of sound, the calyx of Held terminal is capable of sustained, high frequency transmission with high temporal fidelity (Masterton, 1967). Possible functional advantages of heterogeneous release probability with respect to this quality have been discussed in detail by other authors (Wu and Borst, 1999; Sakaba and Neher, 2001b). Very briefly, one concept proposes that vesicles that, by whatever mechanism, have a low chance to be released by a single action potential, may have a higher release probability (RP) in succeeding, high frequency action potentials (~ 100 Hz or more). The increase in RP is thought to be due to the Ca^{2+} (bound or unbound) that remains in the terminal from one or more previous action potentials. The exact mechanism of this facilitation of the RP is not crucial to the concept (for a review on facilitation, see Zucker, 1999). A gradual increase in RP would enable the synapse to maintain release during high frequency firing without 'losing' the majority of releasable vesicles during the first few action potentials already.

D.4.2.1. Modeling trains of action potentials

In our model, RP is heterogeneous due to a non-uniform location of vesicles across different release sites of the same terminal. We will now illustrate how this can lead to a gradual increase in RP during high frequency firing. As our model simulates the calcium dynamics of the entire terminal (see section B.2.2.3) it predicts a rise in the volume average [Ca^{2+}] during each action potential (Figure D-5, right axis). To include the effect of calcium removal, we added to the model a linear extrusion mechanism with a rate $\gamma = 900\ sec^{-1}$ (as measured for

the calyx of Held; Helmchen et al., 1997). The model, including all parameters, was kept unchanged otherwise. I_{Ca} prompted by successive action potentials remained unchanged. This is in line with the above concept, which assumes that possible changes in I_{Ca} during high frequency trains are not the main factor for increasing RP.

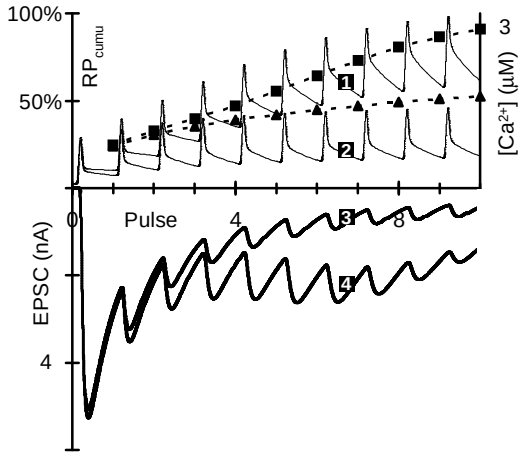

Figure D-5. Functional significance: High frequency transmission.
Release during high frequency transmission (Release Model A). 1: volume average $[Ca^{2+}]$ in terminal (right axis) during 10 consecutive action potentials (200 Hz) ('low-buffer', endogenous fixed buffer and ATP only). 2: as trace 1 but with additional 0.5 mM EGTA ('high-buffer'). 3: EPSC for high-buffer terminal; 4: EPSC for low-buffer terminal; squares: cumulative number of vesicles released after each pulse in the control terminal (as fraction of readily releasable pool at start of train); triangles: as squares but for buffered terminal. Ca^{2+} extrusion included (see text). Results illustrate the functional advantage of heterogeneous release probability in maintaining high frequency synaptic transmission.

Figure D-5 shows predicted phasic transmitter release during a 200 Hz train of 10 consecutive action potentials. We will compare two situations: (1) Release predicted for the native terminal, i.e. with only endogenous buffers in the presynaptic solution (henceforth low-buffer terminal). (2) Release predicted for a terminal dialyzed with 0.5 mM EGTA (henceforth high-buffer terminal). In the following, $RP(i)_{cumu}$ denotes the cumulative number of vesicles released up to the i-th action potential (AP(i)), divided by the total number of vesicles available for release at the start of the train. Comparing the incremental release from AP to AP, we extract the release probability per single action potential $RP(i)_{single}$, which denotes the number of vesicles released by AP(i) divided by the total number of vesicles available for release prior to AP(i). $RP(i)_{single}$ is thus the average RP of those vesicles that have remained in the terminal after all APs prior to AP(i). Note that the EPSCs in Figure D-5 are calculated assuming a linear superposition of quantal responses. This leads to a deviation

from experimental EPSCs, particularly during the decay phase of single EPSCs and during trains (Sakaba and Neher, 2001b). Therefore, we focus our analysis on the number of released vesicles, but nevertheless include the EPSC for illustration of the concept.

D.4.2.2. Non-physiological, high-buffer scenario

For the high-buffer terminal, the fraction of vesicles released after the first action potential is $RP(1)_{cumu} = 24.0\%$. $RP(2)_{cumu} = 30.8\%$, $RP(3)_{cumu} = 35.4\%$ (Figure D-5). For the following APs, $RP(i)_{cumu}$ increases to $RP(10)_{cumu} = 52.8\%$, meaning that after the 10th AP about half of the readily releasable vesicles in the original terminal have been released. Again for the high buffer terminal, $RP(1)_{single} = 24.0\%$, $RP(2)_{single} = 9.0\%$, $RP(3)_{single} = 6.7\%$, and it decreases to $RP(10)_{single} = 3.6\%$. The decrease in $RP(i)_{single}$ for consecutive action potentials is expected because the release probability is heterogeneous. During each action potential, the good vesicles are preferentially released (in our case good means located close to the channel-cluster) whereas the bad ones (i.e. further from channel-cluster) tend to be left behind. Such a decrease in the release probability during the first few stimuli of a train has been measured at the calyx of Held terminal (Sakaba and Neher, 2001b). The predicted volume average $[Ca^{2+}]_{vol}$ rises only moderately during the course of 10 action potentials: from 0.23 μM after the first AP (near spatial equilibrium) to 0.63 μM after the tenth AP. Therefore – in line with the above concept – any facilitation is kept to a minimum and the increase in $RP(i)_{single}$ during the train of action potentials does not occur in the high-buffer terminal.

D.4.2.3. Physiological, low-buffer scenario

For the low-buffer terminal, the situation is quite different. $RP(1)_{cumu} = 24.9\%$. $RP(2)_{cumu} = 32.9\%$, $RP(3)_{cumu} = 39.8\%$. $RP(i)_{cumu}$ increases to $RP(10)_{cumu} = 91.1\%$, meaning that after the 10th AP almost all of the vesicles in the original terminal have been released (Figure D-5). In contrast to the high buffer terminal, the volume average $[Ca^{2+}]_{vol}$ rises significantly from 0.33 μM after the first AP to 2.19 μM after the tenth AP – in line with the above concept. (After 10 action potentials, 120 μM Ca^{2+} (10 APs with 12 μM each) have entered the terminal, of which 72 μM were extruded and 46 μM were buffered.) $RP(1)_{single} = 24.9\%$, $RP(2)_{single} = 10.7\%$, $RP(3)_{single} = 10.3\%$. However, after the third AP, the release probability increases again. $RP(4)_{single} = 12.3\%$, $RP(5)_{single} = 15.8\%$, and $RP(i)_{single}$ steadily increases to $RP(10)_{single} = 33.0\%$. The gradual increase in $RP(i)_{single}$ allows the model synapse to make use of the vesicles not released during the first action potentials (due to disadvantageous location),

such that the number of quanta released during action potential 4 - 8 is stabile. The EPSC amplitude decreases for APs 9 and 10. This is because the pool of releasable vesicles in the original terminal is almost exhausted. $RP(10)_{cumu}$ = 91.1% implies that the terminal could not maintain transmission beyond 50 µsec (10 action potentials). However, at 50 msec, experiments for the calyx of Held have measured significant recruitment of new vesicles, i.e. vesicles that were not yet included in the original count of readily releasable vesicles (Wu and Borst 1999). Even if these vesicles had a rather low response to single, isolated action potentials (due to either intrinsic properties or their disadvantageous location), they could be facilitated in the above fashion (see discussion in Wu and Borst 1999). Therefore, in a realistic terminal, such rapidly recruited, new vesicles will be available to maintain release of neurotransmitter during high frequency transmission (Wang and Kaczmarek, 1998; Dittmann et al., 2000).

D.4.2.4. Mechanisms of facilitation in the model

We will now focus on the response to the second action potential. In the low buffer terminal, $RP(2)_{single}$ = 10.7%, whereas this probability is somewhat lower (9.0%) in the high buffer terminal. A lower $RP(2)_{single}$ in the presence of buffers, i.e. a more pronounced heterogeneity, has in fact been measured for the calyx of Held (Sakaba and Neher, 2001b). 10.7% vs. 9.0% implies a facilitation of RP of ~ 20% (comparing low buffer vs. high buffer terminal). In our model, the facilitation of vesicles during consecutive action potentials is caused by several effects: (1) Ca^{2+} still bound to binding sites of release controlling molecular sensor after first action potential (marginal contribution, off-rates are fast) (2) pre-equilibration of the release controlling molecular sensor to a higher volume average $[Ca^{2+}]_{vol}$ (marginal contribution); (3) partial saturation (local and global) of endogenous buffers (fixed and ATP) and therefore less effective attenuation of the local $[Ca^{2+}]$ transients for the second AP (moderate contribution; but see discussion in Neher, 1998a, and Bennett et al., 2000); (4) higher $[Ca^{2+}]_{local}$ transients during the second AP because transients induced by I_{Ca} are added (approximately) to the higher volume average $[Ca^{2+}]_{vol}$ at the start of the second AP (main contribution). Note that we do not claim that these effects describe facilitation of physiological release probabilities in a more than qualitative way. Nor do we hereby exclude the possibility of additional mechanisms responsible for short term facilitation at the calyx of Held terminal. In experiments using trains of action potentials, the second EPSC and thus the implied $RP(2)_{single}$ is higher than that predicted by our model (Schneggenburger et al., 1999). We therefore

believe, that there are additional mechanisms contributing to short term facilitation which are not yet captured by the model.

E. SUMMARY AND DISCUSSION OF RESULTS

E.1. ROBUSTNESS OF CONCLUSIONS AND SENSITIVITY TO POORLY KNOWN PARAMETERS

The main result we present regards the functional topography of release sites at a calyx of Held at the developmental stage postnatal day 8 - 10: (A) The majority of calcium channels that control phasic release follows a high degree of spatial order. Channels are spatially organized in tight clusters (10 or more channels per cluster, cluster diameter ~ 50 nm or less). (B) Readily releasable vesicles are located at heterogeneous distance from the channel cluster that controls their release (distance ranging between 30 nm and 300 nm, average distance ~ 100 nm). However, we do not exclude the possibility of other distributions of vesicle distance – provided they are not equidistant – as these may result in similar, net release across all release sites of the terminal (see example in conclusion I).

E.1.1. Findings on release site topography are robust

The above result is based on detailed analysis, both quantitative and qualitative, of a large body of experimental data of the calyx of Held. We arrived at each of the conclusions I - III based on robust quantitative effects regarding the modulation of phasic transmitter release by various experimental techniques and their implication for the relative location of channels and vesicles that would explain the experimental results. Conclusion I - III were deduced largely independently: I regards the heterogeneous distance of vesicles from release controlling calcium sources (based on the differential effect of kinetically fast vs. slow buffers); II regards primarily the relative location of calcium sources (based on dose-dependent effects of individual calcium buffers); III regards the topographical design of individual calcium sources as clusters of multiple channels (based on the effects of reducing the number of functional channels). Using the heterogeneous release site topography proposed in chapter D, the model's predictions for phasic release probability are in good agreement with experimental data. Note that the simulations for dose-dependent exogenous buffer effects (Figure D-3 B), for lowered extra cellular [Ca^{2+}] (Figure C-3 D), and for reduced channel open probability (Figure C-3 C, N = 12) use a single, consistent model. All parameters in these scenarios are the same, except for the ones varied to simulate the experimental condition (concentration of exogenous buffers, single channel conductance, and action potential waveform, respectively).

The above conclusions are insensitive to the exact choice of parameters underlying the quantitative modeling. Conclusion I is independent of the exact distribution of distances assumed between vesicles and release controlling calcium sources (simple distribution 0 - 125 nm vs. distribution function appreciating varying sizes of individual active zones). Also, conclusion I is independent of the exact time course of I_{Ca}. The scenario assuming a pulse-like I_{Ca} of 100 µsec duration (Figure D-4) yields 33% release probability for the control condition, 21% for 10 mM EGTA, and 11% for the 1 mM BAPTA condition (relative effect on release as experimentally observed). Conclusion II holds true for BAPTA and both parameter sets for EGTA. It is independent of the inclusion of the calcium buffer ATP in the terminal. Conclusion III can be arrived at independently of the buffered diffusion of calcium (see simplified model). Predicted release probabilities, which are the basis for conclusions I - III, show only small sensitivity to any reasonable variations of the kinetic parameters of endogenous buffers. Finally, conclusions I - III were tested with two kinetic models quantifying the calcium sensitivity and time course of phasic transmitter release at the calyx of Held.

E.1.2. Findings on calcium transients depend on release model

An additional result we present regards the amplitudes of $[Ca^{2+}]$ transients that drive phasic transmitter release during physiological action potentials at the calyx of Held synapse. These we cannot quantify with certainty. Since the two kinetic release models each ascribe different intrinsic calcium sensitivities to the pool of readily releasable vesicles, the prediction of exact amplitudes depends on which model is used in the calculation (Figure D-2 A versus C). In line with recent estimates for this synapse, the amplitudes of the $[Ca^{2+}]$ transients are lower than previously assumed, i.e. tens of µM rather than hundreds of µM (Schneggenburger and Neher, 2000; Bollmann et al., 2000). Depending on their distance to the channel cluster, vesicles are exposed to peak amplitudes ranging between 1 µM and 60 µM. These concentrations are much lower than those required to cause significant local depletion of mobile buffers such as BAPTA. Therefore, such 'buffer-saturation' no longer appears to be the mechanism underlying the observed differential effects of BAPTA versus EGTA in suppressing phasic release (see Naraghi and Neher, 1997). As for the time course of $[Ca^{2+}]$ transients that control phasic release, we have shown that they follow the time course of I_{Ca}, with only a small lag of about 50 µsec (except for the few vesicles located further than

~ 150 nm away). The small lag, however, is aided by the tight clustering of calcium channels as explained above.

E.2. IMPLICATIONS OF RESULTS WITH REGARD TO OTHER, RELATED STUDIES

E.2.1. Non release-controlling Ca^{2+} channels and channel sub-types

In our model, a fraction of the calcium channels in the presynaptic membrane (58% - 83%) do not directly control phasic release but contribute to volume average [Ca^{2+}] only (see section D.1.4). This design of the model is supported by studies using immuno-staining of Ca^{2+} channels at the calyx of Held. Whereas most P/Q-type Ca^{2+} channels appear to be located near release sites only, part of the N-type and R-type channels appear to be located hundreds of nanometers away from active zones, including on the presynaptic membrane opposite the synaptic cleft (Wu et al., 1999). The role of different sub-types of calcium channels in triggering phasic transmitter release has been shown to shift during early development of the calyx of Held (postnatal day 7-13). The contribution of N-type and R-type channels decreases, leaving P/Q-type as the predominant Ca^{2+} channel sub-type to trigger phasic release (Iwasaki and Takahashi, 2000). We therefore believe that the Ca^{2+} channel clusters in our model – which mediate the local [Ca^{2+}] signal for phasic release – are best viewed as representing P/Q-type channel clusters at active zones at the calyx of Held.

E.2.2. Possible other causes for heterogeneous release probability

Heterogeneous release probability of vesicles has been observed at several synapses of the central nervous system. The heterogeneity was found either across terminals of the same type, with each terminal probably involving a single or a few release sites (Markram et al., 1997; Dobrunz and Stevens, 1997); or across release sites within the same terminal (Silver, 1998). Release probability was found to be continuous and broadly distributed, thus not indicating the existence of discrete sub-classes of release probability. At the calyx of Held, which combines 1000 - 2000 release sites into a single, giant-type terminal, it was recently measured that the (phasic) release probability of different release sites within the same terminal is heterogeneous (Sakaba and Neher, 2001b). There is a multitude of possible mechanisms that can cause individual, releasable vesicles to have different chances of being released during an action potential (for discussion see Sakaba and Neher, 2001b). Here we propose that the heterogeneity may be caused to a large extent by the variability in the distance between a vesicle and its release controlling channel cluster. Other, intrinsic

properties of the release controlling molecular sensor and the fusion machinery, in particular their sensitivity to identical [Ca^{2+}] transients, are either the same or contribute to a lesser extent to the measured heterogeneity. Our argument for this is twofold: (1) At the calyx of Held, the calcium sensitivity of release has been measured by using spatially homogeneous [Ca^{2+}] signals uncaged from photo-sensitive chelators. The kinetics of fast transmitter release – measured over a large range of [Ca^{2+}] – could be well explained by a single kinetic model for all vesicles in the readily releasable pool (Schneggenburger and Neher, 2000; Bollmann et al., 2000). These studies may be interpreted as indicating that intrinsic heterogeneities of the vesicles response to [Ca^{2+}] are marginal. (Note that possible evidence for a heterogeneity was observed only for vesicles that do not contribute to the fast/phasic component of transmitter release; Schneggenburger and Neher, 2000). (2) Although it is not usually measurable during single action potentials, the heterogeneity of the release probability literally appears when the terminal is dialyzed with exogenous buffers that have different binding kinetics for calcium (BAPTA vs. EGTA, see conclusion I). Such buffers differentially modify the [Ca^{2+}] transients during action potentials, the main difference being at what distance from the calcium channels they are most potent in attenuating the amplitude of the transient. Thus it seems likely that the observed heterogeneity of the release probability, to a large extent, is mediated by the distance between vesicles and calcium channels itself. As shown, this assumption accurately predicts the experimental results. (For a discussion of possible other sources of differential effects of BAPTA vs. EGTA, see Rozov et al., 2001.) However, we cannot exclude a significant presence of additional, intrinsic heterogeneity in the release probability. Such heterogeneity would aid to explain experimental results of exogenous buffers in a similar fashion.

E.2.3. Possible higher spatial organization

The heterogeneous topography we propose bears important implications for the mechanism by which readily releasable vesicles and calcium channels are spatially organized at active zones at the calyx of Held. Whereas the Ca^{2+} channels controlling phasic release appear to be closely clustered (conclusion IV), our model did not assume any preferential location of vesicles with respect to the Ca^{2+} channels. Instead, vesicles were located at random anywhere on the active zone. Hypothetical anatomical links between some or all vesicles to Ca^{2+} channels would modify the random distribution of distance, possibly creating distinct sub-classes of vesicles. Such a possibility has been discussed recently for another central synapse

(Rozov et a., 2001). When compared to experimental data, our analysis did not indicate the existence of such vesicle-classes or any other mechanism to directly control the distance between vesicles and Ca^{2+} channels at the calyx of Held (other than their confinement to active zones). However, we cannot generally exclude such a mechanism since we cannot conclude the exact distribution of vesicle distance (see above). Recently, the heterogeneity of release probability at the calyx of Held has been shown to be modifiable by additions of cyclic AMP (cAMP) to the presynaptic solution. A possible explanation for this effect is that cAMP modifies the number of vesicles located close to release controlling channels (Sakaba and Neher, 2001a).

E.3. FUNCTIONAL ADVANTAGE OF PROPOSED TOPOGRAPHY

E.3.1. Synaptic fidelity and heterogeneous location of vesicles

The rather loose and non-uniform spatial organization of vesicles and Ca^{2+} channels we propose for the central synapse we studied is in stark contrast to that of the neuromuscular junction of crayfish (Msghina, 1999), squid (Adler et al., 1991) and frog. At the frog's neuromuscular junction, Ca^{2+} channels and vesicles are arranged at active zones in a highly organized fashion, resulting in a homogenous distance of only ~ 10 nm between vesicles and their closest channels (Harlow et al., 2001). However, non-uniform location of vesicles at the calyx of Held offers crucial functional advantages for the specific transmission characteristics of this synapse. As shown, the multitude of vesicles' distances to channels – in our model simply random – serves to create an immediate back-up pool of vesicles which become gradually available for release during high frequency firing.

E.3.2. Synaptic fidelity and clustering of release controlling channels

Controlling phasic transmitter release by more than one calcium channel per vesicle ('domain overlap') offers several advantages over a single channel regime. This is particularly relevant in the case of fast firing synapses such as the calyx of Held (for discussion, see Borst and Sakmann, 1999a). We have shown that the topographical organization of release sites at this synapse features an especially strong case of domain overlap: Vesicles are not merely controlled by a loose group of calcium channels, each of them located at different distances from the vesicle. Instead, release controlling channels are probably organized in tight clusters, featuring ten or more channels per cluster which occupy only a small space (diameter not more than ~ 50 nm). As shown in Conclusion III,

this feature essentially ensures that the stochastic gating of voltage gated calcium channels generates a nevertheless reliable and low-noise [Ca^{2+}] transient controlling the release of transmitter (discussed in Stanley, 1997). Recent studies for the calyx of Held synapse have found that a further increase in its maximum firing rate during early development (postnatal day 5 - 14) may in part be aided by a more rapid time course of the presynaptic action potential (Taschenberger and von Gersdorff, 2000). A more rapid AP, however, only results in a more rapid [Ca^{2+}] transient for individual vesicles[44] if a closely grouped cluster of many channels controls each vesicle. The clustering of calcium channels thus ensures maximum benefit of more rapid APs for the fidelity of synaptic transmission.

Concluding, we find that crucial characteristics of synaptic transmission of this central synapse are facilitated by the particular topographic organization of calcium channels and vesicles at its release sites. Spatially highly organized clusters of calcium channels control the release of vesicles whose locations with respect to the clusters vary, thus providing for functionally advantageous, heterogeneous release probability. The developmental specialization of this synapse towards high fidelity, high frequency transmission may be aided by a fundamental spatial re-organization of its release sites toward the described topography.

[44] For non-clustered, or fewer calcium channels, only the *average* calcium signal would benefit from a more rapid action potential, not however the individual signal controlling any particular vesicle during a single action potential (see explanations in section C.4).

References

Adler EM, Augustine GJ, Duffy SN, Charlton MP (1991) Alien intracellular calcium chelators attenuate neurotransmitter release at the squid giant synapse. J Neurosci 11:1496-1507.

Allbritton NL, Meyer T, Stryer L (1992) Range of messenger action of calcium ion and inositol 1,4,5-triphosphate. Science 258:1812-1815.

Artalejo CR, Adams ME, Fox AP (1994) Three types of Ca^{2+} channels trigger secretion with different efficacies in chromaffin cells. Nature 367:72-76.

Augustine GJ, Adler EM, Charlton MP (1991) The calcium signal for transmitter secretion from presynaptic nerve terminals. Ann NY Acad Sci 635:365-381.

Augustine GJ and Neher E (1992) Neuronal [Ca^{2+}] signalling takes the local route. Current Opinion in Neurobiology 2:302-307.

Barrett EF, Stevens CF (1972) The kinetics of transmitter release at the frog neuromuscular junction. J Physiol (Lond) 227:691-708.

Baylor SM, Hollingworth S (1998) Model of sarcomeric Ca^{2+} movements, including ATP Ca^{2+} binding and diffusion, during activation of frog sceletal muscle. J Gen Physiol 112:297-316.

Bennett MR, Farnell L, Gibson WG (2000) The probability of quantal secretion near an array of calcium channels of an active zone. Biophys J 78:2222-2240

Bertram R, Smith GD, Sherman A (1999) Modeling study of the effects of overlapping Ca^{2+} microdomains on neurotransmitter release. Biophys J 76:735-750.

Bollmann JH, Sakmann B, Borst JGG (2000) Calcium sensitivity of glutamate release in a calyx-type terminal. Science 289:953-957.

Borst JGG, Helmchen F, Sakmann B (1995) Pre- and postsynaptic whole-cell recordings in the medial nucleus of the trapezoid body of the rat. J Physiol 489:825-840.

Borst JGG, Sakmann B (1996) Calcium influx and transmitter release in a fast CNS synapse. Nature 383:431-434.

Borst JGG, Sakmann B (1998) Calcium current during single action potential in a large presynaptic terminal of the rat brain stem. J Physiol 506:143-157.

Borst JGG, Sakmann B (1999a) Effects of changes in action potential shape on calcium currents and transmitter release in a calyx-type synapse of the rat auditory brain stem. Phil Trans R Soc London 354:347-355

Borst JGG, Sakmann B (1999b) Depletion of calcium in the synaptic cleft of a calyx-type synapse in the rat brainstem. J Physiol 521:123-133.

Chow RH, Klingauf J, Neher E (1994) Time course of Ca^{2+} concentration triggering exocytosis in neuroendocrine cells. PNAS 91:12765-12769.

Cooper RL, Winslow JL, Govind CK, Atwood HL (1996) Synaptic structural complexity as a factor enhancing probability of calcium-mediated transmitter release. J Neurophysiol 75:2451-2466.

DiGregorio DA, Peskoff A, Vergara JL (1999) Measurement of action potential-induced presynaptic calclium domains at a cultured neuromuscular junction. J Neurosci 19:7846-7859.

Dittmann JS., Kreitzer AC, Regehr WG (2000) Interplay between facilitation, depression, and residual calcium at three presynaptic terminals. J Neurosci 20: 1374-1385.

Dobrunz LE, Stevens CF (1997) Heterogeneity of release probability, facilitation, and depletion at central synapses. Neuron 18:995-1008.

Forsythe ID (1994) Direct patch recording from identified presynaptic terminals mediating glutamatergic EPSCs in the rate CNS, in vitro. Journal of Physiology 479:381-387.

Gil A, Segura J, Pertusa JAG, Soria B (2000) Monte Carlo Simulation of 3-d buffered Ca^{2+} diffusion in neuroendocrine cells. Biophys J 78:13-33.

Golasch M, Hescheler J, Quale JM, Patlak JB, Nelson MT (1992) Single calcium channel currents of arterial smooth muscle at physiological calcium concentrations. Am J Physiol 263: C948-C952.

Harlow LH, Ress D, Stoschek A, Marshall RM, McMahan UJ (2001) The architecture of active zone material at the frog's neuromuscular junction. Nature 409:479-484.

Helmchen F, Borst JGG, Sakmann B (1997) Calcium dynamics associated with a single action potential in a CNS presynaptic terminal. Biophys J 72:1458-1471.

Iwasaki S, Momiyama A, Uchitel OD, Takahashi T (2000) Developmental changes in calcium channel types mediating central synaptic transmission. J Neurosci 20:59-65.

Katz B. *The Release of Neural Transmitter Substances* (Thomas, Springfield, IL, 1969).

Klingauf J, Neher E (1997) Modeling buffered Ca^{2+} diffusion near the membrane: implications for secretion in neuroendocrine cells. Biophys J 72:674-690.

Llinas R, Sugimori M, Silver RB (1992) Microdomains of high calcium concentration in a presynaptic terminal. Science 256:677-679

Lübke, Frotscher, Borst, Söhl, Eils, Saracoglu, Roth, Sätzler, Sakmann (2001) to be submitted

Markram H, Lübke J, Frotscher M, Roth A, Sakmann B (1997) Physiology and anatomy of synaptic connections between thick tufted pyramidal neurones in the developing rat neocortex. J Physiol 500:409-440.

Masterton B, Jane JA, Diamond IT (1967) Role of brain stem auditory structures in sound localization. I. Trapezoid body, superior olive, and lateral lemniscus. J Neurophysiol 30:341-359.

Matthews G (2000) Vesicle fiesta at the synapse. Nature 406:835-836.

Morest DK (1968) The growth of synaptic endings in the mammalian brain: a study of the calyces of the trapezoid body. Zeitschrift für Anatomie und Entwicklungsgeschichte 127:201-220.

Msghina M, Millar AG, Charlton MP, Govind CK, Atwood HL (1999) Calcium entry related to active zones and differences in transmitter release at phasic and tonic synapses. J Neurosci 19:8419-8434.

Nägerl UV, Novo D, Mody I, Vergara JL (2000) Binding kinetics of calbindin-D_{28k} determined by flash photolysis of caged Ca^{2+}. Biophys J 79:3009-3018.

Naraghi M (1997) T-jump study of calcium binding kinetics of calcium chelators. Cell Calcium 22:255-268.

Naraghi M, Neher E (1997) Linearized buffered Ca^{2+} diffusion in microdomains and its implications for calculation of $[Ca^{2+}]$ at the mouth of a calcium channel. J Neurosci 17:6961-6973.

Neher E (1986) Concentration profiles of intracellular calcium in the presence of a diffusible chelator. In: Calcium electrogenesis and neuronal functioning (Heinemann U, Klee M, Neher E, Singer W, eds), pp 80-96. Berlin: Springer.

Neher E (1998a) Usefulness and limitations of linear approximations to the understanding of Ca^{++} signals. Cell Calcium 24:345-357.

Neher E (1998b) Vesicle pools and Ca^{2+} microdomains: New tools for understanding their roles in neurotransmitter release. Neuron 20:389-399.

W.H. Press, S.A. Teukolsky, W.T. Vetterling, and B.P. Flannery, Numerical Recipes in C (Cambridge; Cambridge University Press, 1988).

Quastel DMJ, Guan YY, Saint DA (1992) The relation between transmitter release and Ca^{2+} entry at the mouse motor nerve terminal: Role of stochastic factors causing heterogeneity. Neuroscience 51:657-671.

Roberts WM, Jacobs RA, Hudspeth AJ (1990) Colocalization of ion channels involved in frequency selectivity and synaptic transmission at presynaptic active zones of hair cells J Neurosci 10:3554-3684.

Roberts WM (1994) Localization of calcium signals by a mobile calcium buffer in frog saccular hair cells. J Neurosci 14:3246-3262.

Rowland KC, Irby NK, Spirou AG (2000) Specialized synapse-associated structures within the calyx of Held. J Neurosci 20:9135-9144.

Rozov A, Burnashev N, Sakmann B, Neher E (2001) Title subject to change. Journal of Physiology xx, in press

Sakaba T, Neher E (2001a) Preferential potentiation of fast-releasing synaptic vesicles by cAMP at the calyx of Held. PNAS 98:331-336.

Sakaba T, Neher E (2001b) Quantitative relationship between transmitter release and calcium current at the calyx of Held synapse. J Neurosci 15 Jan 2001.

Schneggenburger R, Meyer AC, Neher E (1999) Released fraction and total size of pool of immediately available transmitter quanta at a calyx synapse. Neuron 23:399-409.

Schneggenburger R, Neger E (2000) Intracellular calcium dependence of transmitter release rates at a fast central synapse. Nature 406:889-893.

Silver RA, Momiyama A, Cull-Candy SG (1998) Locus of frequency dependent depression identified with multiple-probability fluctuation analysis at rat climbing fibre-Purkinje cell synapses. J Physiol (London) 510:881-902.

Smith GD. Modeling local and global calcium signals using reaction diffusion equations. In: *Computational Neuroscience* (CRC Press, Boca Raton, FL, 2001)

Stanley EF (1997) The calcium channel and the organization of the presynaptic transmitter release face. Trends Neurosci 20:404-409.

Sugimori M, Lang EJ, Silver RB, Llinas R (1994) High-resolution measurement of the time course of calcium-concentration microdomains at squid presynaptic terminal. Biol Bull 187:300-303.

Taschenberger H, von Gersdorff H (2000) Fine-tuning an auditory synapse for speed and fidelity: Developmental changes in presynaptic waveform, EPSC kinetics, and synaptic plasticity. J Neurosci 20:9162-9173.

Tucker T, Fettiplace R (1995) Confocal imaging of calcium microdomains and calcium extrusion in turtle hair cells. Neuron 15:1323:1336.

Wagner J, Keizer J (1994) Effects of rapid buffers in Ca^{2+} diffusion and Ca^{2+} oscillations. Biophys J 67:447-456.

Wang LY, Kaczmarek LK (1998) High-frequency firing helps replenish the readily releasable pool of synaptic vesicles. Nature 394:384-388.

Wu LG, Borst JGG (1999) The reduced release probability of releasable vesicles during recovery from short-term synaptic depression. Neuron 23:821-832.

Wu LG, Westenbroek RE, Borst JGG, Catterall WA, Bert Sakmann (1999) Calcium channel types with distinct presynaptic localization couple differentially to transmitter release in single calyx-type synapses. J Neurosci 19:726-736.

Yamada WM, Zucker RS (1992) Time course of transmitter release calculated from simulations of a calcium diffusion model. Biophys J 61:671-682.

Zucker RS, Fogelson AL (1986) Relationship between transmitter release and presynaptic calcium influx when calcium enters through discrete channels. PNAS 83:3032-3036.

Zucker RS, Stockbridge N (1983) Presynaptic calcium diffusion and the time course of transmitter release and synaptic facilitation at the squid giant synapse. J. Neurosci 3:1263-1269.

Zucker RS (1999) Calcium- and activity-dependent synaptic plasticity. Curr Opin Neurobiol 9:305-313.